Recent Advances in Chlorine, Bromine, and Iodine Solid-State NMR Spectroscopy

Patrick M.J. Szell, David L. Bryce
Department of Chemistry, University of Ottawa, Ottawa, Ontario, Canada

Contents

Abstract

We survey the latest advances in quadrupolar halogen ($^{35/37}$Cl, $^{79/81}$Br, and ^{127}I) solid-state nuclear magnetic resonance (SSNMR). The reporting period is from August 2008 through to July 2014; prior work has been covered in a previous review from our group (Widdifield *et al.* [2]). The past 6 years have witnessed a continued growth in the areas of application of chlorine, bromine, and iodine SSNMR. Such areas include the study of halogen-bonded adducts, pharmaceutical polymorphs, inorganic compounds and materials, supported catalysts, ionic liquids, glasses, and more. Many of the new studies focus on the $^{35/37}$Cl nuclides due to their relatively favorable spectroscopic properties compared to the $^{79/81}$Br and ^{127}I nuclides. The first systematic $^{35/37}$Cl SSNMR studies of covalently bonded chlorine in organic and inorganic compounds have been reported. Higher applied magnetic fields and ongoing technique development continue to open new avenues of opportunity for applications of chlorine, bromine, and iodine SSNMR.

Keywords: Chlorine-35, Chlorine-37, Bromine-79, Bromine-81, Iodine-127, Quadrupolar nuclei, Solid-state NMR, Halogens

Annual Reports on NMR Spectroscopy
ISSN 0066-4103
http://dx.doi.org/10.1016/bs.arnmr.2014.10.002

ABBREVIATIONS

BRAIN broadband adiabatic inversion
Cp cyclopentadienyl
Cp* pentamethylcyclopentadienyl
C_Q nuclear quadrupolar coupling constant
CS chemical shift
CSA chemical shift anisotropy
CT central transition
DFT density functional theory
EFG electric field gradient
GIPAW gauge-including projector-augmented wave
IUPAC International Union of Pure and Applied Chemistry
MAS magic-angle spinning
N.A. natural abundance
NQR nuclear quadrupole resonance
QCPMG quadrupolar Carr–Purcell Meiboom–Gill
QUEST QUadrupolar Exact SofTware
SSNMR solid-state nuclear magnetic resonance
VOCS variable-offset cumulative spectrum
WURST wideband uniform rate and smooth truncation
δ_{11}, δ_{22}, δ_{33} principal components of the chemical shift tensor
δ_{iso} isotropic chemical shift
η_Q quadrupolar asymmetry parameter
κ skew of the chemical shift tensor
ν_0 Larmor frequency
ν_Q quadrupolar frequency
Ω chemical shift tensor span

1. INTRODUCTION

Chlorine-35/37, bromine-79/81, and iodine-127 are all quadrupolar nuclei with good natural abundances (N.A.) and reasonably high magnetogyric ratios (Table 1). Due to their quadrupolar nature ($I=3/2$ for ^{35}Cl, ^{37}Cl, ^{79}Br, and ^{81}Br; $I=5/2$ for ^{127}I), broad nuclear magnetic resonance (NMR) powder patterns are expected in the solid state for all but the most symmetric of coordination environments. In this *Annual Report*, we provide a survey of the literature from the period covering August 2008 to July 2014. Our previous reviews [1–3], in particular a previous *Annual Report* published in 2009 [2], offer a broader review of the literature covering prior years. An *Encyclopedia of Magnetic Resonance* article offers a more pedagogical perspective [4]. Butler *et al.* have also provided a review of literature covering both solid-state and solution-phase data [5].

Table 1 NMR properties of the half-integer spin quadrupolar halogen nuclei

	N.A. (%)	I	Q (mb)	$\Delta\nu_{CT}$ (Rel.)	Ξ (%)	$\gamma/10^7$ (rad $T^{-1}s^{-1}$)
^{35}Cl	75.78	3/2	−81.65(80)	1.340	9.797909	2.624198
^{37}Cl	24.22	3/2	−64.35(64)	1.000	8.155725	2.184368
^{79}Br	50.69	3/2	313(3)	7.702	25.053980	6.725616
^{81}Br	49.31	3/2	261.5(25)	5.006	27.006518	7.249776
^{127}I	100.0	5/2	−696(12)	11.445	20.007486	5.389573
^{211}At	–	9/2	–	–	–	–

Table 2 Recommended chemical shift standards for $^{35/37}Cl$, $^{79/81}Br$, and ^{127}I solid-state NMR

	IUPAC primary standard[a]	SSNMR secondary standard[b]	Secondary chemical shift (ppm)[b,c]
$^{35/37}Cl$	0.1 mol/dm^3 NaCl	NaCl(s)	−41.11
		KCl(s)	8.54
^{79}Br	0.01 mol/dm^3 NaBr	NaBr(s)	1.29
		KBr(s)	54.31
^{81}Br	0.01 mol/dm^3 NaBr	NaBr(s)	1.57
		KBr(s)	54.51
^{127}I	0.01 mol/dm^3 KI	NaI(s)	226.71
		KI(s)	192.62

[a]Harris *et al.* (in D_2O) [6].
[b]Bryce and coworkers [2,4].
[c]With respect to primary standard at 0 ppm.

Given this previous coverage, here we aim to keep our focus on the reporting period, and largely avoid repeating previous information and references. The NMR properties of the quadrupolar halogens are shown in Table 1, and the primary and secondary chemical shift (CS) references are presented in Table 2. Further information on CS referencing may be found in Refs. [2,4].

Following a short section describing some basic parameter definitions and information on spectral line shape modeling, the chapter is broken down into three additional sections describing new chlorine, bromine, and iodine data and results. Each of these sections also presents, in tabular form, the new

CS and quadrupolar coupling data published during the reporting period. This is followed by some brief concluding remarks.

2. THEORY AND MODELING

The theory relevant to the description of the NMR spectra of the quadrupolar halogens has been given previously [2,3]. We present here only some of the useful definitions and key equations, along with a brief discussion on some aspects of the modeling of spectra of powdered samples.

2.1. Interactions and Definitions

The majority of the studies covered in this report are on microcrystalline powdered samples. The NMR line shape of a quadrupolar nucleus such as $^{35/37}$Cl, $^{79/81}$Br, or ^{127}I in a powdered sample is determined by perturbations to the Zeeman interaction originating largely from the nuclear electric quadrupolar interaction. The quadrupolar interaction is that between the nuclear electric quadrupolar moment (Q) and the electric field gradient (EFG) at the nucleus. The EFG is described by a second-rank tensor, V, which can be diagonalized to give three principal components ($|V_{33}| \geq |V_{22}| \geq |V_{11}|$). The magnitude of the traceless quadrupolar coupling tensor is typically described by two parameters, namely the quadrupolar coupling constant (C_Q),

$$C_Q = \frac{eQV_{33}}{h}$$

and the quadrupolar asymmetry parameter,

$$\eta_Q = \frac{(V_{11} - V_{22})}{V_{33}}.$$

The value of η_Q ranges from zero (no asymmetry) to one. The quadrupolar interaction almost always dominates the NMR spectra of $^{35/37}$Cl, $^{79/81}$Br, and ^{127}I. In a perfectly symmetric environment (e.g., O_h or T_d symmetry), both C_Q and η_Q will be zero, indicating a lack of EFG. In lower-symmetry environments, C_Q will be nonzero. The value of η_Q, as suggested by its name, is an indicator of the asymmetry of the EFG, with a value of zero indicating at least axial symmetry and a value of unity indicating maximum asymmetry of the EFG tensor.

The magnetic shielding of the nucleus gives rise to a CS. Both the magnetic shielding and the CS are generally anisotropic. The NMR spectra of

$^{35/37}$Cl, $^{79/81}$Br, and ^{127}I therefore also depend on their CS. The CS may be represented as a second-rank tensor, the magnitude of which may be described by the following parameters in its principal axis system (principal components are given by $\delta_{11} \geq \delta_{22} \geq \delta_{33}$).

$$\text{Isotropic chemical shift}: \quad \delta_{\text{iso}} = \left(\frac{1}{3}\right)(\delta_{11} + \delta_{22} + \delta_{33})$$

$$\text{Span}: \quad \Omega \approx \delta_{11} - \delta_{33}$$

$$\text{Skew}: \quad \kappa = \frac{3(\delta_{22} - \delta_{\text{iso}})}{\Omega}$$

Note that in all of the data tables in this report, the CSs are listed as referenced in the original literature, with footnotes explaining the references used. While desirable, it can be difficult to put all literature data on a common scale with high accuracy, because sometimes the references used are at different concentrations, temperatures, in different solvents, or there is simply not enough information reported to properly convert between shift scales. For this reason, we have not attempted to convert literature data.

In principle, the solid-state NMR (SSNMR) spectra of $^{35/37}$Cl, $^{79/81}$Br, and ^{127}I are also affected by spin–spin coupling interactions including direct dipolar coupling and indirect nuclear spin–spin coupling (J coupling). The effects of these interactions are very often too small to observe for systems of interest; a few studies have focussed on these small effects in recent years and are mentioned in the following sections. For the majority of the cases discussed herein, the spectra are dominated by the quadrupolar interaction, and in some cases, it has proven possible to measure chemical shift anisotropy (CSA) as well. CSs and CSAs may be interpreted in terms of the electronic and molecular structure.

2.2. Second-Order Perturbation Theory versus an Exact Treatment of the Quadrupolar Interaction

The quadrupolar interaction is typically treated as a perturbation, to second order, of the dominant Zeeman interaction when describing the SSNMR spectra of quadrupolar nuclei. This approach has been enormously successful. For nuclei with particularly strong quadrupolar interactions, however, it is not surprising that this perturbation theoretical approach may break down under appropriate conditions (i.e., where the quadrupolar frequency (ν_{Q}) becomes comparable to the Larmor frequency (ν_0)). During the reporting period, quadrupolar halogen SSNMR studies have provided valuable

experimental data for the assessment of the limits of second-order perturbation theory in describing the NMR line shapes of quadrupolar nuclei. Widdifield and Bryce noted in a ^{127}I SSNMR study of a series of alkaline earth metal iodides that standard second-order perturbation theory could not properly model some of the spectra [7]. It was noted that the discrepancies between experiment and theory vanished when carrying out the experiments in a higher applied magnetic field. Furthermore, experiments on barium iodide, which contains two crystallographically distinct iodine sites, showed the discrepancies only for the site with the larger quadrupolar interaction, and not for the site with the smaller interaction (see Fig. 1). Informed further by additional independent nuclear quadrupole resonance (NQR) experiments, both of these observations were consistent with a breakdown of second-order perturbation theory. A follow-up study on $^{185/187}$Re SSNMR of perrhenates allowed for the establishment of rules of thumb for the safe interpretation of SSNMR spectra of spin-5/2 nuclei (such as ^{127}I) in powdered samples [8]. The errors in the derived spectral parameters depend on the ratio of ν_0 to ν_Q (ν_Q is equal to $3C_Q/20$ for a spin-5/2 nucleus when $\eta_Q = 0$). The error in the measured CS in particular increases quite rapidly as the ν_0/ν_Q ratio drops (see Fig. 2). It is very important to be aware of such potential errors when fitting the powder patterns of quadrupolar nuclei that are subject to strong quadrupolar interactions.

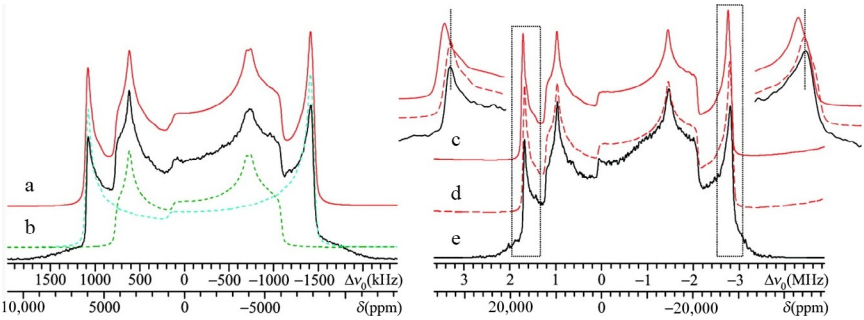

Figure 1 Analytical simulations (a, c and d) and experimental static VOCS Solomon echo (b and e) ^{127}I SSNMR spectra of powdered BaI_2, acquired at (b) 21.1 T and (e) 11.75 T. A deconvolution is shown via the dotted traces in (b). The spectra inset above (c) correspond to the regions within the dotted boxes. They highlight the detectable deviation in the apparent chemical shift, when comparing analytical simulations at 11.75 and 21.1 T. This discrepancy is due to orientation-dependent higher-order quadrupolar-induced effects. *Reprinted with permission from Ref. [7]. Copyright 2010 American Chemical Society.*

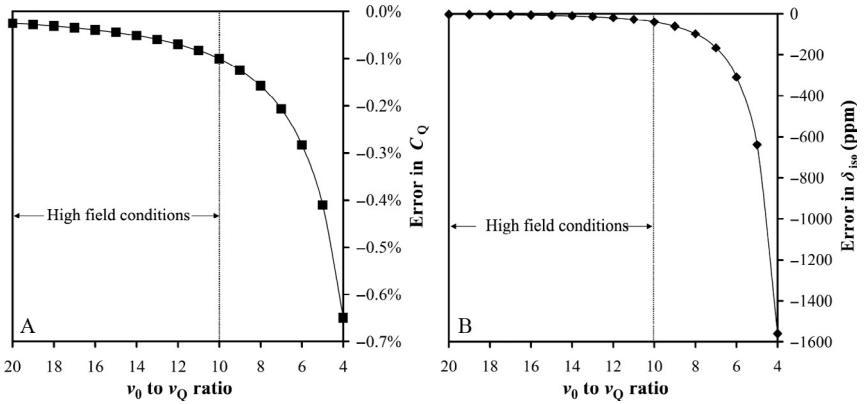

Figure 2 Illustrations of the errors associated with using second-order perturbation theory to model SSNMR line shapes for the case where $I = 5/2$ and $\eta_Q = 0$, relative to an exact simulation. (a) Error in the C_Q value as a function of the ν_0/ν_Q ratio and (b) error in the isotropic chemical shift as a function of the same ratio. *From Ref. [8]. Reproduced by permission of the PCCP Owner Societies.*

To overcome possible errors in the derived parameters when fitting NMR spectra of powdered samples with large quadrupolar interactions, Perras *et al.* developed and implemented an exact treatment of the quadrupolar and Zeeman interactions for stationary powdered samples [9]. The software, QUEST (QUadrupolar Exact SofTware), is freely available and produces spectral simulations in a fraction of a second on a modern computer [10]. The importance of this exact treatment was demonstrated in a $^{35/37}$Cl SSNMR study of a series of organic compounds featuring covalent carbon–chlorine bonds [11]. In those cases, it was noted that discrepancies of up to hundreds of kHz in the position of one of the spectral discontinuities were observed if second-order perturbation theory was used rather than an exact treatment, even in a high magnetic field of 21.1 T. There is also a concomitant error in the isotropic chemical shift on the order of 600 ppm.

3. SOLID-STATE CHLORINE-35/37 NUCLEAR MAGNETIC RESONANCE

Over the course of the past 6 years, several new developments and applications of $^{35/37}$Cl SSNMR have been reported. Most of these studies have been carried out on powdered samples, and line shape analyses most often yielded information such as the isotropic chemical shift, quadrupolar coupling constant, and quadrupolar asymmetry parameter. In favorable

cases, information on the chlorine chemical shift tensor and the relative orientation of the CS and EFG tensors is also obtained. To obtain the latter information with good precision, it is recommended to acquire spectra in more than one applied magnetic field and of both chlorine isotopes. As for all nuclides, the effect of CSA will be amplified in Hertz in higher applied magnetic fields, while the effect of the second-order quadrupolar broadening will be diminished. Spectral data for the reporting period are summarized in Tables 3–17. Below, we provide an overview of some of the recent work.

Due to the high spherical symmetry of the electron distribution in a closed-shell chloride ion, the majority of the reports continue to focus on the observation of chloride ions in various solid-state environments. Distortion of the environment of the chloride ion from a perfectly cubic site (as found, for example, in alkali metal chlorides) results in a nonzero EFG and measurable quadrupolar parameters. Widdifield and Bryce reported a $^{35/37}$Cl and ^{43}Ca study of anhydrous calcium chloride and its hydrates [17]. It was shown that $^{35/37}$Cl SSNMR was a useful tool to differentiate in particular between anhydrous $CaCl_2$ and $CaCl_2{\cdot}6H_2O$. Older literature values for $CaCl_2$ were corrected in this study, and it was noted that both the chlorine quadrupolar coupling constant and CS decrease upon hydration in this series of hydrates. Complementary gauge-including projector-augmented wave–density functional theory (GIPAW–DFT) computations and ^{43}Ca SSNMR experiments provided additional structural insights into these systems.

Penner *et al.* reported a multinuclear NMR and quantum chemical study of solid trimethylammonium chloride [18]. ^{35}Cl quadrupolar and CS parameters were determined experimentally and were also computed as a function of the proton position in the N–H$\cdots$Cl$^-$ hydrogen bond fragment. The authors conclude that the measured NMR parameters (which also included $^{1/2}$H and $^{14/15}$N NMR data) are consistent with a structure where the hydrogen atom is completely bonded to the nitrogen atom, but which participates in a moderately strong hydrogen bond with the chloride ion.

Chapman *et al.* reported the first study of a chloride anion receptor by $^{35/37}$Cl SSNMR and GIPAW–DFT calculations [19]. The high symmetry of the anion-binding site in the 1-butyl-3-methylimidazolium chloride complex of *meso*-octamethylcalix[4]pyrrole results in a relatively small $C_Q(^{35}\text{Cl})$ value of 1.0 MHz. This paper also reported a systematic study of GIPAW–DFT-computed chlorine NMR parameters for the anion receptor and for a benchmark series of crystalline amino acid hydrochlorides. The calculations were found to systematically overestimate the values of

Table 3 ^{35}Cl SSNMR parameters for HCl pharmaceuticals from Hildebrand *et al.* [12]

Compounds	δ_{iso} (ppm)[a]	Ω (ppm)	$\lvert C_Q(^{35}Cl)\rvert$ (MHz)	η_Q	κ	Notes
Adiphenine hydrochloride	128(5)	155(20)	5.94(6)	0.18(3)	0.60(20)	Experimental
	103	*160*	*−7.34*	*0.14*	*0.84*	*Calculated*[b]
Buflomedil hydrochloride	75(10)	125(30)	5.67(13)	0.18(6)	−0.60(20)	Experimental
	39	*122*	*−7.68*	*0.16*	*−0.15*	*Calculated*
Dicyclomine hydrochloride	52(4)	100(10)	5.80(5)	0.45(1)	0.00(20)	Experimental
	98	*140*	*−7.62*	*0.40*	*−0.15*	*Calculated*
Trigonelline hydrochloride	70(10)	120(30)	7.50(12)	0.05(3)	0.80(20)	Experimental
	84	*194*	*−9.61*	*0.16*	*0.42*	*Calculated*
Ranitidine hydrochloride	75(5)	70(15)	4.70(10)	0.92(3)	0.30(30)	Experimental
	55	*71*	*5.71*	*0.81*	*−0.17*	*Calculated*
Dibucaine hydrochloride site 1	105(15)	100(20)	4.65(20)	0.86(7)	−0.26(60)	Experimental
Scopolamine hydrochloride	0(4)	50(4)	3.82(3)	0.99(1)	−1.00(30)	Experimental
	28	*81*	*5.90*	*0.93*	*−0.30*	*Calculated*
Bromhexine hydrochloride	85(5)	90(10)	5.80(3)	0.04(1)	0.00(10)	Experimental
	116	*126*	*−7.63*	*0.26*	*0.14*	*Calculated*
Alprenolol hydrochloride	60(1)	88(2)	5.25(2)	0.87(1)	0.00(20)	Experimental
	75	*142*	*6.42*	*0.96*	*0.09*	*Calculated*

Continued

Table 3 ^{35}Cl SSNMR parameters for HCl pharmaceuticals from Hildebrand *et al.* [12]—cont'd

Compounds	δ_{iso} (ppm)	Ω (ppm)	$\lvert C_Q(^{35}Cl)\rvert$ (MHz)	η_Q	κ	Notes
Isoprenaline hydrochloride	73(4)	90(3)	5.30(5)	0.93(4)	−1.00(10)	Experimental
	82	*128*	*7.63*	*0.88*	*0.45*	*Calculated*
Acebutolol hydrochloride	95(5)	95(10)	4.57(5)	0.50(4)	−0.30(30)	Experimental
	129	*61*	*−5.51*	*0.81*	*0.32*	*Calculated*
Amantadine hydrochloride	131(5)	50(5)	2.90(4)	0.68(3)	0.60(20)	Experimental
	159	*82*	*3.99*	*0.41*	*−0.35*	*Calculated*
Procainamide hydrochloride	50(2)	60(10)	4.25(5)	0.52(2)	0.00(20)	Experimental
	90	*127*	*−5.17*	*0.85*	*−0.64*	*Calculated*
Dopamine hydrochloride	33(7)	50(14)	5.10(14)	0.74(18)	0.00(50)	Experimental
	83	*94*	*−7.30*	*0.52*	*0.32*	*Calculated*
Aminoguanidine hydrochloride	50(3)	55(5)	2.0(2)	0.76(4)	0.45(15)	Experimental
	92	*84*	*3.37*	*0.38*	*−0.15*	*Calculated*
Isoxsuprine hydrochloride	120(10)	50(20)	5.50(15)	0.25(5)	0.50(40)	Experimental
	104	*52*	*6.75*	*0.17*	*0.32*	*Calculated*
Isoxsuprine hydrochloride site 1	80(3)	120(6)	6.5(1)	0.36(2)	−0.50(20)	Experimental
	112	*46*	*8.60*	*0.34*	*0.62*	*Calculated*

Isoxsuprine hydrochloride site 2	80(4)	175(20)	5.6(1)	0.33(1)	0.00(15)	Experimental
	102	*46*	*7.02*	*0.31*	*0.51*	*Calculated*
Mexiletine hydrochloride site 1	90(5)	80(20)	5.45(10)	0.40(8)	−0.80(20)	Experimental
	77	*109*	*7.23*	*0.29*	*−0.81*	*Calculated*
Mexiletine hydrochloride site 2	130(5)	75(20)	3.10(10)	0.55(10)	0.80(20)	Experimental
	102	*74*	*3.03*	*0.86*	*0.75*	*Calculated*
Mexiletine hydrochloride I	55(4)	30(3)	1.99(10)	0.62(3)	−0.30(10)	Experimental

[a]All chemical shifts were referenced to NaCl(s) at 0.00 ppm.
[b]For calculated values reported in this and subsequent tables, please refer to the original references for computational details. Calculated vales are signed while experimental values are magnitudes only.

Table 4 ^{35}Cl solid-state NMR data for haloanilinium chlorides from Attrell *et al.* [13]

Compounds	δ_{iso} (ppm)[a]	Ω (ppm)	$\lvert C_Q(^{35}Cl)\rvert$ (MHz)	η_Q	κ	Notes
2-Chloroanilinium chloride	70(1)	95(5)	6.04(3)	0.34(1)	−0.20(2)	Experimental
	113.2	*100.2*	*4.21*	*0.42*	*−0.41*	*Calculated*
2-Bromoanilinium chloride	79(1)	95(5)	6.01(1)	0.330(5)	−0.50(2)	Experimental
	132.1	*96.2*	*4.25*	*0.54*	*−0.60*	*Calculated*
2-Iodoanilinium chloride	75(1)	40(5)	2.12(2)	0.76(1)	−0.10(2)	Experimental
3-Chloroanilinium chloride	88(1)	100(5)	5.30(5)	0.025(5)	−0.80(1)	Experimental
	136.2	*94.5*	*3.83*	*0.13*	*−0.65*	*Calculated*
3-Bromoanilinium chloride	85(1)	95(10)	5.37(3)	0.025(5)	−1.0(0.1)	Experimental
3-Iodoanilinium chloride	77(1)	90(5)	5.39(5)	0.02(2)	−0.50(2)	Experimental
4-Chloroanilinium chloride	69(1)	115(5)	6.02(5)	0.56(1)	−1.0(0.1)	Experimental
	124.7	*74.0*	*3.43*	*0.65*	*−0.38*	*Calculated*
4-Bromoanilinium chloride	67(1)	90(5)	5.60(5)	0.60(1)	−0.40(1)	Experimental
	102.6	*78.1*	*3.91*	*0.69*	*0.07*	*Calculated*
4-Iodoanilinium chloride	71(1)	120(5)	4.33(7)	0.38(1)	0.0(0.1)	Experimental
	121.0	*101.0*	*3.36*	*0.34*	*0.26*	*Calculated*

[a]All chemical shifts were referenced to 0.1 mol/dm^3 NaCl in D_2O. Secondary standards were NaCl(s) at −41.11 ppm or KCl(s) at 8.54 ppm.

Table 5 ^{35}Cl SSNMR parameters for pure ionic liquid salts from Gordon *et al.* [14]

Compounds	δ_{iso} (ppm)[a]	$\lvert C_Q(^{35}Cl)\rvert$ (MHz)	η_Q
mbpyri chloride	83.15(0.07)	0.857(0.008)	0.525(0.005)
	70.56(0.04)	0.889(0.008)	0.08(0.08)
bdmim chloride	71.60(0.02)	0.978(0.004)	0.10(0.02)
emim chloride	91.72(0.03)	0.808(0.004)	0.95(0.01)
	74.98(0.04)	0.805(0.005)	0.20(0.02)
	71.36(0.04)	0.884(0.004)	0.86(0.01)
	60.60(0.03)	0.972(0.005)	0.80(0.01)
bmim chloride	71.65(0.05)	1.500(0.002)	0.390(0.005)

[a]All chemical shifts were referenced to 0.1 M NaCl in D_2O. See Fig. 4 for structures of the cations.

$C_Q(^{35}Cl)$, δ_{iso} (^{35}Cl), and Ω (^{35}Cl) relative to the experimental values [31–33]. Such information is useful when attempting to interpret NMR data in cases where the structure is not known *a priori*, or where NMR crystallographic structure refinement protocols are used.

Many pharmaceuticals are prepared as hydrochloride salts for reasons of solubility, crystallinity and/or stability. Schurko and coworkers describe the potential of ^{35}Cl SSNMR spectroscopy as a tool for pharmaceutical hydrochloride polymorph fingerprinting and recognition [12,34]. By examining a large series of samples, it is shown that the chlorine EFG and CS tensors are generally distinct for each pharmaceutical compound, and for each polymorph. The authors also correlate the quadrupolar coupling parameters to the local hydrogen bond environment of the chloride ions and report several trends, some of which corroborate those reported previously [31,35].

Evidence for uptake of chlorine SSNMR spectroscopy by the pharmaceutical industry is found in two published works from researchers at GlaxoSmithKline plc. [28,36]. Vogt *et al.* analyzed a boron-containing antibacterial hydrochloride salt, named (*S*)-3-(aminomethyl)-8-(3-hydroxypropoxy)benzo[*c*][1,2]oxaborol-1(3*H*)-ol hydrochloride [28]. The multinuclear magnetic resonance study indicated the increased potential applications of SSNMR in the pharmaceutical industry, with ^{35}Cl magic-angle spinning (MAS) SSNMR offering direct insight into the chlorine environment and overall crystal structure. Combined with NMR data from other nuclei and DFT calculations, a complete picture of the structure of the drug emerged. The same group studied polymorphism in ethyl 3-{3-[((2*R*)-3-{[2-(2,3-dihydro-1*H*-inden-2-yl)-1,1-dimethylethyl]amino}-

Table 6 ^{35}Cl SSNMR parameters for germanium chloride and related complexes

Compounds	δ_{iso} (ppm)[a]	Ω (ppm)	$\lvert C_Q(^{35}Cl)\rvert$ (MHz)	η_Q	κ	References
$GeCl_2$	75(2)	–	<40 kHz	–	–	Greer *et al.* [15]
$GeCl_2$·dioxane	300(50)	250(100)	28.3(1)	0.055(10)	1	Hanson *et al.* [16]
[NHC]$GeCl_2$	200(50)	300(100)	29.3(1)	0.12(2)	1	[16]
iPr[NHC]$GeCl_2$	150(50)	–	28.6(3)	0.23(5)	–	[16]
2,2′-Bipyridine·$GeCl_2$	200(50)	–	15.3(2)	0.13(2)	–	[16]
	250(50)	250(100)	14.1(1)	0.10(2)	0	
1,10-Phenanthroline·$GeCl_2$	250(50)	200(100)	13.8(1)	0.15(2)	0	[16]
	250(50)	–	29.6(1)	0.18(2)	–	
Benzo-15-cr-5-$GeCl^+$	300(50)	350(100)	25.1(1)	0.10(2)	1	[16]
Dichlorodimesitylgermane	200(100)	–	43.0(5)	0.1(1)	–	[16]
Chlorotrimesitylgermane	200(100)	–	41.5(5)	0	–	[16]
Tin chloride cryptand complex	200(50)	–	19.0(1)	0.15(5)	–	[16]

[a]Chemical shifts were referenced to 1 M KCl in H_2O, except for $GeCl_2$ which was referenced to 1 M NaCl(aq).

Table 7 ^{35}Cl SSNMR parameters for platinum chlorides complexes from Lucier *et al.* [41,42]

Compounds	δ_{iso} (ppm)[a]	$\lvert C_Q(^{35}Cl)\rvert$ (MHz)	η_Q	Notes
K_2PtCl_4	−125(75)	35.7(2)	0.09(1)	WURST–QCPMG
$Pt(NH_3)_4Cl_2{\cdot}H_2O$	100(5)	1.85(5)	0.30(5)	Hahn-echo
Magnus' green salt $[Pt(NH_3)_4][PtCl_4]$	−125(75)	35.6(2)	0.095(10)	WURST–QCPMG
Magnus' pink salt $[Pt(NH_3)_4][PtCl_4]$	0(75) 0(75)	33.8(2) 35.1(1)	0.11(1) 0.10(1)	Site 1 Site 2; WURST–QCPMG
cis-$PtCl_2(NH_3)_2$	–	33.8(2)	0.20(1)	Site 1; $\Omega = 650(300)$ ppm
	–	32.8(2)	0.15(1)	Site 2; $\Omega = 650(300)$ ppm
	–	34.6(2)	0.21(1)	Site 3; $\Omega = 650(300)$ ppm
trans-$PtCl_2(NH_3)_2$	–	37.3(1)	0.12(1)	$\Omega = 650(300)$ ppm

[a]Chemical shifts are referenced to NaCl(s) ($\delta_{iso} = 0.0$ ppm).

Table 8 ^{35}Cl SSNMR parameters for calcium chloride and its hydrates from Widdifield and Bryce [17]

Compounds	δ_{iso} (ppm) [a]	Ω (ppm)	$\lvert C_Q(^{35}Cl)\rvert$ (MHz)	η_Q	κ	Notes
Anhydrous $CaCl_2$	122(5)	–	2.1(1)	0.7(1)	–	Experimental
	105(8)	135 (15)	8.82(8)	0.383 (15)	0.0(3)	Experimental
	179.0	*200.9*	*9.66*	*0.419*	0.12	*Calculated*
$CaCl_2{\cdot}2H_2O$	69(2)	72(15)	4.26(3)	0.75(3)	0.6(2)	Experimental
	109.3	*140.7*	*4.43*	*0.520*	*0.49*	*Calculated*
α-$CaCl_2{\cdot}4H_2O$	*76.1*	*73.6*	*−3.70*	*0.405*	*0.39*	*Calculated*
	78.7	*77.9*	*5.97*	*0.944*	*−0.47*	*Calculated*
β-$CaCl_2{\cdot}4H_2O$	*92.9*	*123.5*	*−3.75*	*0.947*	*0.70*	*Calculated*
	78.9	*83.6*	*2.16*	*0.828*	*0.59*	*Calculated*
	104.6	*125.6*	*3.97*	*0.776*	*0.45*	*Calculated*
γ-$CaCl_2{\cdot}4H_2O$	*48.5*	*77.1*	*3.59*	*0.149*	*0.12*	*Calculated*
$CaCl_2{\cdot}6H_2O$	57(3)	40(8)	4.33(3)	<0.01	*−1*	Experimental
	43.3	*46.4*	*5.48*	*0.000*	*−1*	*Calculated*

[a]All chemical shifts were referenced to 0.1 mol/dm^3 of NaCl in D_2O ($\delta_{iso} = 0$ ppm) using solid KCl as a secondary reference.

Table 9 ^{35}Cl SSNMR parameters for trimethylammonium chloride at variable conditions from Penner *et al.* [18]

Compounds	δ_{iso} (ppm)[a]	Ω (ppm)	$\lvert C_Q(^{35}Cl)\rvert$ (MHz)	η_Q	κ	T (K)
Trimethylammonium chloride ($B_0 = 11.75$ T)	32(5)	56 (35)	5.54 (0.03)	0.05 (0.04)	−0.42(0.10)	295
Trimethylammonium chloride ($B_0 = 18.8$ T)	35(5)	47 (25)	5.59 (0.03)	0.04 (0.02)	−0.53(0.16)	295
Trimethylammonium chloride-*d*1 ($B_0 = 18.8$ T)	34(5)	48 (30)	5.30 (0.02)	0.06 (0.04)	−0.42(0.10)	295
Trimethylammonium chloride ($B_0 = 11.75$ T)	27(7)	47 (20)	5.44 (0.10)	0.01 (0.01)	−1.0[b]	330

[a]All chemical shifts were referenced to NaCl(s) and then corrected by subtracting 45.37 ppm.
[b]Lower limit. This value can vary from −0.75 to −1.0 without affecting the simulated line shape.

2-hydroxypropyl)oxy]-4,5-difluorophenyl}propanoate hydrochloride using multinuclear SSNMR, including ^{35}Cl MAS studies [36]. Two different forms of the pharmaceutical compound yielded distinguishable ^{35}Cl MAS NMR spectra, demonstrating the value of the technique in an industrial setting. Despite the increased application of ^{35}Cl SSNMR in the pharmaceutical industry for elucidating polymorphism, certain constraints such as disorder and overlapped second-order quadrupolar patterns may complicate the interpretation of spectra and limit the precision of the information that can be extracted.

Halogen SSNMR has proven to be an important tool in characterizing the electronic and chemical environment within halogen-bonded compounds [13,23,37,38]. A halogen bond, RX···Y, is the result of an electrostatic interaction between an electron donor (Y) and the electrophilic region of a halogen (X). A series of haloanilium halides featuring weak halogen bonds has been analyzed by ^{35}Cl, ^{81}Br, and ^{127}I SSNMR and their δ_{iso} and C_Q values have been reported in order to determine the relationship between the local halogen bond geometry and the NMR observables [13]. In this study, the electron donors (halide ions) were probed via NMR, as the quadrupolar interactions of the covalently bonded halogens are typically prohibitively large [1,2]. Interpretation of the experimental data in concert with GIPAW–DFT calculations revealed several trends (see Table 4). For example, in isostructural series, the halide quadrupolar coupling constant was found to increase as the halogen bond weakens. Viger-Gravel *et al.* recently reported a comprehensive study of halogen bonds via SSNMR

Table 10 ^{35}Cl SSNMR parameters for amino acid hydrochlorides from Chapman *et al.* [19]

Compounds	δ_{iso} (ppm)[a]	Ω (ppm)	$\lvert C_Q(^{35}Cl)\rvert$ (MHz)	η_Q	κ	Notes
Alanine hydrochloride	106(5)	60(30)	6.4(0.1)	0.75(0.06)	−0.3(0.5)	Experimental
	146	*75*	*8.45*	*0.775*	*0*	*Calculated*
Arginine hydrochloride	91.5(1.0)	57.5(3.0)	2.035(0.020)	0.98(0.02)	0.27(0.10)	Experimental
	51	*44*	*2.45*	*0.197*	*−0.2*	*Calculated*
Aspartic acid hydrochloride	102(5)	75(30)	7.1(0.1)	0.42(0.05)	−0.9(0.1)	Experimental
	149	*91*	*10.31*	*0.396*	*−0.7*	*Calculated*
Cysteine hydrochloride	104.2(0.5)	66(10)	3.92(0.01)	0.47(0.02)	0.12(0.12)	Experimental
	155	*86*	*4.00*	*0.505*	*0.1*	*Calculated*
Glutamic acid hydrochloride	102(1)	66(15)	3.61(0.01)	0.65(0.02)	0.0(0.3)	Experimental
	142	*84*	*4.3*	*0.30*	*0.3*	*Calculated*
Glycine hydrochloride	101(5)	100(20)	6.42(0.05)	0.61(0.03)	0.3(0.3)	Experimental
	133	*110*	*8.14*	*0.80*	*0.3*	*Calculated*
Histidine hydrochloride	93(1)	<150	4.59(0.03)	0.46(0.02)	–	Experimental
	112	*99*	*2.72*	*0.716*	*−0.5*	*Calculated*
Lysine hydrochloride	105(2)	26(10)	2.49(0.01)	0.42(0.02)	−0.4(0.4)	Experimental
	107	*54*	*4.41*	*0.77*	*−0.2*	*Calculated*

Continued

Table 10 ^{35}Cl SSNMR parameters for amino acid hydrochlorides from Chapman *et al.* [19]—cont'd

Compounds	δ_{iso} (ppm)	Ω (ppm)	$\lvert C_Q(^{35}Cl)\rvert$ (MHz)	η_Q	κ	Notes
Methionine hydrochloride	99(1)	100(20)	4.41(0.02)	0.35(0.03)	0.3(0.3)	Experimental
	138	*137*	*6.20*	*0.375*	*0.2*	*Calculated*
Phenylalanine hydrochloride	96(5)	129(20)	6.08(0.05)	0.52(0.03)	0.26(0.25)	Experimental
	129	*147*	*7.71*	*0.55*	*0.1*	*Calculated*
Proline hydrochloride	37(5)	63(5)	4.50(0.05)	0.63(0.05)	−0.54(0.08)	Experimental
	110	*105*	*9.23*	*0.906*	*0.4*	*Calculated*
Threonine hydrochloride	99(10)	95(40)	5.4(0.1)	0.94(0.02)	−0.2(0.5)	Experimental
	149	*133*	*12.21*	*0.849*	*0.2*	*Calculated*
Tryptophan hydrochloride	105(1)	72(5)	5.05(0.04)	0.86(0.03)	0.1(0.1)	Experimental
	151	*127*	*11.62*	*0.816*	*0.5*	*Calculated*
Tyrosine hydrochloride	94.7(0.5)	<150	2.23(0.02)	0.72(0.03)	–	Experimental
	142	*129*	*3.27*	*0.35*	*−0.5*	*Calculated*
Valine hydrochloride	90(10)	125(40)	5.89(0.05)	0.51(0.005)	0.35(0.5)	Experimental
	128	*149*	*7.96*	*0.55*	*0.1*	*Calculated*

[a]All chemical shifts were referenced to NaCl(s) ($\delta_{iso} = 0$ ppm).

Table 11 ^{35}Cl SSNMR parameters for organometallic complexes from Rossini *et al.* [20]

Compounds	δ_{iso} (ppm)[a]	$\lvert C_Q(^{35}Cl)\rvert$ (MHz)	η_Q
Cp_2TiCl_2	500(500)	22.1(5)	0.61(3)
Cp_2ZrCl_2	300(150)	16.0(5)	0.72(4)
Cp_2HfCl_2	400(500)	17.1(4)	0.65(5)
$Cp^*_2ZrCl_2$	400(400)	16.7(4)	0.73(3)
$CpTiCl_3$	500(150)	15.5(4)	0.54(5)
$Cp_2ZrMeCl$	400(400)	13.7(4)	0.75(10)
$(Cp_2ZrCl)_2\mu$-O	300(400)	16.3(4)	0.43(7)
Cp^*ZrCl_3	400(200)	12.8(5)	0.10(10)
	400(200)	13.3(5)	0.12(10)
	200(200)	14.6(5)	0.88(10)
	200(200)	14.0(5)	0.80(10)
$CpZrCl_3$[b]	300	14.8–18.6	0.7–0.8
CpZrHCl	80(50)	19.7(3)	0.20(4)

[a]All chemical shifts were referenced using NaCl(s) for which δ_{iso} was −45.37 ppm with respect to an infinitely dilute solution of NaCl(aq).
[b]Multiple sites.

and molecular orbital analyses [23]. Among other findings, the sensitivity of the ^{35}Cl quadrupolar parameters to the wide range of possible halogen bond geometries in a series of perfluoroiodobenzene-onium halide salts was demonstrated. A natural localized molecular orbital (NLMO) analysis provided a simple picture connecting the magnitude of the quadrupolar interaction with the strength of the C–I$\cdots$Cl$^-$ halogen bond via a lone pair orbital centered on the chloride ion. This work also demonstrated a commonality between the geometrical dependence of quadrupolar asymmetry parameters measured for electron donors in halogen bonds (^{35}Cl, ^{81}Br) and that established previously for hydrogen bonds (^{17}O) (see Fig. 3).

Ionic liquids have attracted much attention in recent years, with many potential applications such as tunable organic solvents. A range of pure ionic liquid salts has been studied using liquid-state and solid-state NMR by Gordon *et al.* [14]. ^{35}Cl, ^{79}Br, and ^{127}I SSNMR were used to probe these molecules to extract information on the solid phase (see Fig. 4 for structures and Table 5 for data). Relaxation times were measured, and second-order quadrupolar coupling was used to investigate molecular motions.

Table 12 ^{35}Cl SSNMR parameters for covalently bound chlorine from Perras and Bryce [11]

Compounds		δ_{iso} (ppm)[a]	$\lvert C_Q(^{35}Cl)\rvert$ (MHz)	η_Q
5-Chlorouracil		300(50)	−75.03(0.05)	0.096(0.002)
2-Chloroacetamide		150(50)	−68.30(0.05)	0.031(0.003)
Sodium chloroacetate		150(50)	−67.75(0.05)	0.022(0.002)
α,α′-Dichloro-*o*-xylene		200(50)	−66.43(0.08)	0.008(0.003)
Chlorothiazide		350(50)	−73.04(0.08)	0.139(0.002)
2,4′-Dichloroacetophenone (diuril)		150(100)[b]	−70.70(0.08)[b]	0.032(0.003)[b]
		350(100)[c]	−68.65(0.08)[c]	0.111(0.003)[c]
p-Chlorophenylalanine	Site 1	350(100)	−69.0(0.2)	0.093(0.003)
	Site 2	300(150)	−69.5(0.2)	0.073(0.003)

[a]Referenced to KCl(aq).
[b]Bonded to CH_2 group.
[c]Bonded to phenyl ring.

Incorporation mechanisms of chlorine in peralkaline and peraluminous Na_2O–CaO–Al_2O_3–SiO_2 glasses have been studied by multinuclear magnetic resonance, including ^{35}Cl studies (see Table 16) [24]. These systems are models for phonolitic melts. Low concentrations of Cl in some samples, as well as the size and distribution of EFGs, resulted in the limits of sensitivity of ^{35}Cl MAS NMR being tested. Clear differences in the Cl environment were nevertheless identified (see Table 16 for data). ^{35}Cl MAS NMR spectra of peraluminous glasses showed a larger CS distribution and a more positive CS (about −75 ppm) than the peralkaline glasses (about −100 ppm). Peraluminous glasses were also found to be characterized by larger ^{35}Cl quadrupolar coupling constants with a larger distribution, indicating greater disorder in these glasses. In systems such as these, featuring potentially large C_Q values, a distribution in these values, and a low Cl concentration, one must be aware of the possibility of "invisible" chlorine sites, which are simply not seen under typical ^{35}Cl SSNMR conditions.

Crystalline inorganic compounds with metal–chloride bonds have been investigated by Chapman and Bryce [21]. A series of solid anhydrous group 13 chlorides (aluminium trichloride, gallium trichloride, indium trichloride, and gallium dichloride) were studied by high-field variable-offset quadrupolar Carr–Purcell Meiboom–Gill (QCPMG) $^{35/37}$Cl SSNMR (see Table 13). The ^{35}Cl quadrupolar interactions are large in such

Table 13 ^{35}Cl SSNMR for group 13 chlorides from Chapman and Bryce [21]

Compounds	δ_{iso} (ppm)[a]	Ω (ppm)	$\lvert C_Q(^{35}Cl)\rvert$ (MHz)	η_Q	κ	Notes
Aluminium trichloride	325(100)	300(200)	22.5(1.0)	0.63(0.10)	−0.5(0.5)	
Gallium trichloride	200(100)	–	40.4(2.0)	0.03(0.03)	–	Terminal
	150(100)	–	38.1(2.0)	0.09(0.05)	–	Terminal
	250(100)	–	28.3(2.0)	0.48(0.05)	–	Bridging
Gallium dichloride	200(100)	200(200)	31.2(0.7)	0.15(0.15)	−0.5(0.5)	
	200(100)	200(200)	32.0(0.7)	0.20(0.20)	−0.5(0.5)	
Indium trichloride	500(100)	500(200)	24.5(1.0)	0.52(0.10)	0.5(0.5)	

[a]All chemical shifts are referenced to NaCl(s) at 0 ppm.

Table 14 ^{35}Cl SSNMR data for organometallic complexes from Johnston *et al.* [22]

Compounds	δ_{iso} (ppm)[a]	Ω (ppm)	$\lvert C_Q(^{35}Cl)\rvert$ (MHz)	η_Q	κ	Notes
Allylpalladium chloride dimer [{Pd(C_3H_5)Cl}$_2$]	900(100)	500(200)	17.85(10)	0.48(2)	0.99(2)	
Bis(2-methylallyl)palladium chloride dimer [{Pd(C_4H_7)Cl}$_2$]	720(200)	450(200)	16.85(10)	0.48(1)	0.99(2)	
Methallylnickel chloride dimer [{Ni(C_4H_7Cl}$_2$]	−450(200)	600(200)	15.30(10)	0.49(1)	0.99(2)	
Chloronorbornadiene rhodium dimer [{Rh(C_7H_8)Cl}$_2$]	800(100)	750(200)	14.45(20)	0.44(4)	0.99(2)	
Chlorobis(ethylene) rhodium(I) dimer [{Rh(C_4H_8Cl}$_2$]	600(200)	–	21.00(20)	0.23(2)	–	Site 1
	550(200)	–	21.70(20)	0.29(3)	–	Site 2
Chloro-1,5-cyclooctadiene rhodium(I) dimer [{Rh(C_8H_{12})Cl}$_2$]	780(100)	500(100)	16.10(20)	0.44(3)	0.99(1)	
Chloro-1,5-cyclooctadiene iridium(I) dimer [{Ir(C_8H_{12})Cl}$_2$]	1700(200)	–	25.50(40)	0.24(1)	–	Site 1
	1700(200)	–	25.90(30)	0.29(2)	–	Site 2
Dichloro(norbornadiene) palladium(II) [Pd(C_7H_8)Cl]	1100(200)	–	32.00(40)	0.21(4)	–	Site 1
	1100(200)	–	32.50(50)	0.25(3)	–	Site 2
Dichloro(1,5-cyclooctadiene) palladium(II) [Pd(C_8H_{12})Cl_2]	1100(300)	–	36.90(40)	0.18(5)	–	Site 1
	1100(300)	–	37.30(50)	0.23(2)	–	Site 2
Dichloro(1,5-cyclooctadiene) platinum(II), [Pt(C_8H_{12})Cl_2]	1000(300)	–	38.60(50)	0.25(3)	–	Site 1
	1000(300)	–	39.00(40)	0.25(3)	–	Site 2
Dichlorobis(acetonitrile) palladium [Pd(CH_3CN)$_2Cl_2$]	0(100)	–	39.80(20)	0.14(2)	–	

Dichloro(pentamethylcyclopentadienyl) rhodium(III) dimer $[\{Rh(C_{10}H_{15})Cl_2\}_2]$	800(300)	–	26.40(20)	0.49(3)	–	Site 1
	900(200)	–	30.12(40)	0.08(2)	–	Site 2
Dichloro(pentamethylcyclopentadienyl) iridium(III)dimer $[\{Ir(C_{10}H_{15})Cl_2\}_2]$	800(300)	–	30.30(30)	0.62(2)	–	Site 1
	1000(300)	–	35.10(30)	0.09(3)	–	Site 2
Dichloro(benzene) ruthenium(II) dimer $[\{Ru(C_6H_6)Cl_2\}_2]$	800(300)	–	28.40(30)	0.50(3)	–	Site 1
	1000(200)	–	30.90(30)	0.13(3)	–	Site 2
Silica supported $TiCl_4$	700(200)	–	14.31(20)	0.15(5)	–	

[a]All chemical shifts were referenced to 1 M NaCl(aq) using solid NaCl as a secondary reference.

Table 15 ^{35}Cl SSNMR parameters for halogen-bonded compounds from Viger-Gravel *et al.* [23]

Compounds[a]	δ_{iso} (ppm)[b]	Ω (ppm)	$\lvert C_Q(^{35}Cl)\rvert$ (MHz)	η_Q	κ	Notes
(n-Bu_4NCl)(p-DITFB)	117(3)	94(4)	5.43(0.05)	1.00(0.01)	−0.3(0.2)	
(n-Bu_4PCl)(p-DITFB)	132(4)	180(15)	10.42(0.04)	0.07(0.01)	0.85(0.10)	
(n-Bu_4PCl)(o-DITFB)	112(10)	<60	4.57(0.20)	1.00(0.04)	–	Site 1
	148(20)	<60	8.22(0.30)	0.12(0.04)	–	Site 2
	135(20)	<60	7.15(0.05)	0.70(0.04)	–	Site 3
(Ph_4PCl)(p-DITFB)	177(8)	60(15)	3.66(0.10)	0.38(0.04)	−0.4(0.2)	Site 1
	98(4)	96(10)	6.85(0.10)	0.12(0.02)	0.0(0.2)	Site 2
(Ph_4PCl)(o-DITFB)·$2CH_2Cl_2$	94(10)	60(20)	6.77(0.20)	0.44(0.04)	1.00(0.04)	

[a] *p*-DITFB, *para*-diiodotetrafluorobenzene; *o*-DITFB, *ortho*-diiodotetrafluorobenzene.
[b] All chemical shifts were referenced to KCl(s) (δ_{iso} = 8.54 ppm) with respect to 0.1 M NaCl in D_2O.

Table 16 ^{35}Cl SSNMR parameters for peralkaline, peraluminous, and sodium silicates from Baasner *et al.* [24]

Compounds[a]	δ_{iso} (ppm)[b]	$\lvert C_Q(^{35}Cl)\rvert$ (MHz)
Peralkaline		
NACS 1.0F 1.0Cl	−105	2.3
NACS 1.1 Cl + NACS 1.9 Cl	−95	2.8
Peraluminous		
ANCS 1.0F 0.9Cl	−74	3.1
ANCS 0.6Cl + ANCS 1.2Cl	−75	3.0
Sodium silicate		
NS 2.2Cl	−101	2.6

[a]The original reference contains further information about line widths and distributions of the NMR parameters used for spectral fitting.
[b]All chemical shifts were referenced using NaCl(s) ($\delta_{iso} = -46$ ppm) relative to 1 M aqueous NaCl.

compounds where the chlorine–metal bond is largely covalent, relative to those found for chloride ions in hydrochloride salts or glasses as discussed above. The quadrupolar interaction dominates the central transition (CT) in all cases, but in three cases the chlorine chemical shift tensors were also characterized. $C_Q(^{35}Cl)$ values ranged from 22.45 to 40.44 MHz, and the CT spectral breadths ranged from 1.0 to 2.5 MHz at 21.1 T. Chapman and Bryce reported that terminal chlorine sites exhibit larger chlorine C_Q values than do the bridging chlorines, consistent with older NQR literature. Isotropic chlorine CSs were found to range from 150 ± 100 to 375 ± 100 ppm, while the largest chlorine CS tensor span reported in this study is 500 ± 200 for anhydrous $InCl_3$. The chlorine CS increases with the metal–chlorine distance in all cases. Finally, GIPAW calculations are in excellent agreement with experiment, to within 7% in all cases.

Schurko and coworkers have also reported ^{35}Cl studies on a series of group IV transition metal organometallic complexes (Cp_2TiCl_2, $CpTiCl_3$, Cp_2ZrCl_2, Cp_2HfCl_2, $Cp^*_2ZrCl_2$, $CpZrCl_3$, Cp^*ZrCl_3, $Cp_2ZrMeCl$, $Cp_2ZrCl_2\mu$-O, and Cp_2ZrHCl; Cp, cyclopentadienyl; Cp*, pentamethylcyclopentadienyl) yielding quadrupolar coupling, and CS tensor information (Table 11) [20]. Additional investigations using a NLMO analysis were employed to understand the origins of the observed C_Q values. EFG and chemical shift tensor parameters were demonstrated to be sensitive probes of metallocene structure, and allowed for the differentiation of

Table 17 ^{35}Cl SSNMR parameters for additional compounds

Compounds	δ_{iso} (ppm)	$\lvert C_Q(^{35}Cl)\rvert$ (MHz)	η_Q	Comments	References
Hexachlorophene	–	72.1(0.3)	0.08(0.01)		Terskikh *et al.* [25]
B-chlorocatecholborane	50(50)[a]	−41.9(0.1)	0.25(0.03)	Experimental	Perras and Bryce [26]
	120	*−41.3*	*0.27*	*Calculated*	
Trichloroborazine	200(50)	−39.2(0.1)	0.335(0.005)	Site 1	Perras and Bryce [27]
	200(50)	−38.9(1)	0.250(0.005)	Site 2	
(*S*)-3-(Aminomethyl)-7-(3-hydroxypropoxy)benzo[*c*][1,2]oxaborol-1(3*H*)-ol hydrochloride	24.14[b]	5.66	0.90		Vogt *et al.* [28]
$[Nb_6Cl_{12}(OH)_2][(H_2O)_4]\cdot 4H_2O$[c]	628.3	17.18	0.606	Site 1 GIPAW	Perić *et al.* [29]
	617.0	16.00	0.727	Site 2 GIPAW	
	522.0	15.53	0.777	Site 3 GIPAW	
	562.0	15.45	0.791	Site 4 GIPAW	
	543.3	15.60	0.623	Site 5 GIPAW	
	604.0	15.91	0.650	Site 6 GIPAW	
meso-Octamethylcalix[4]pyrrole 1-butyl-3-methyl imidazolium chloride	120(10)[d]	1.0(0.1)	0.7(0.1)		Chapman *et al.* [19]
$ClBuPPh_3$	88.5(0.5)[e]	1.13(0.01)	0.65(0.01)		Burgess *et al.* [30]
		0.88(0.01)[f]			

[a]Referenced with respect to dilute Cl^- using NaCl(s) as a secondary reference at −41.11 ppm.
[b]Experimentally referenced with solid NaCl at 0.0 ppm. The reported isotropic chemical shift value was mathematically corrected to use dilute aqueous NaCl using δ(NaCl at infinite dilution) = δ(NaCl(s) − 45.37 ppm).
[c]Referenced indirectly to the ^{35}Cl resonance of 1 M NaCl(aq) in H_2O. These GIPAW values were found to provide simulations in agreement with the experimental spectrum.
[d]Referenced to NaCl(s) at 0.0 ppm.
[e]Referenced to NaCl(s) at 0.00 ppm.
[f]C_Q measured for ^{37}Cl.

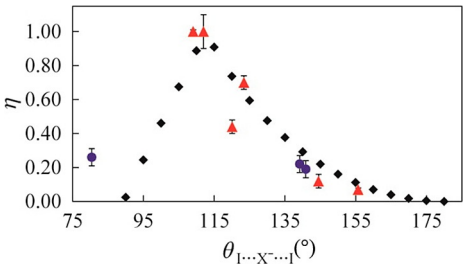

Figure 3 Plot of quadrupolar asymmetry parameter of the central anion versus I···X^{-}···I angle in halogen-bonded systems. The black diamonds represent the calculated values for ^{35}Cl in a F_3C–I···Cl^{-}···I–CF_3 model system. The red (gray in the print version) triangles and blue (dark gray in the print version) circles represent the experimental values for ^{35}Cl and ^{81}Br, respectively. *From Ref. [23]. Copyright 2014 American Chemical Society.*

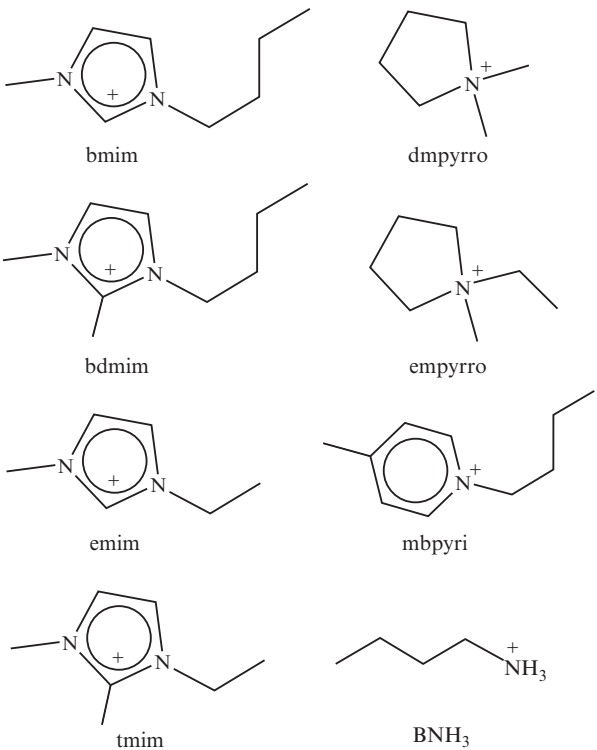

Figure 4 Structures of the cations of ionic liquid salts studied by Gordon *et al.* and their abbreviations. *From Ref. [14]. Copyright Wiley-VCH. Used with permission.*

monomeric and oligomeric structures. First principles calculations of the EFG parameters successfully reproduced the experimental values and trends. Importantly, their results show that while the value of $C_Q(^{35}Cl)$ is sensitive to whether the chlorine is in a terminal or in a bridging position, the relative magnitudes of $C_Q(^{35}Cl)$ for such sites do not always follow the same trend.

The same group has reported further ^{35}Cl SSNMR and NQR studies on additional transition metal organometallic complexes with commonly occurring metal–chlorine bonding motifs (see Table 14) [22]. A range of terminal and bridging chlorine environments in Pd, Rh, Ir, and Ru complexes were investigated. Chlorine EFG and CS tensor parameters were readily extracted from multifield wideband uniform rate and smooth truncation (WURST)–QCPMG data. Again, the quadrupolar parameters were shown to be sensitive to structural differences, and in particular were shown to differentiate easily between chlorine atoms in bridging and terminal bonding environments. DFT calculations of the NMR parameters were consistently in good agreement with the experiment. A final interesting experimental result reported in this work, for $TiCl_4$ supported on silica material, follows up on related work by Hermans and coworkers [39,40], and suggests the applicability of ^{35}Cl SSNMR methods for the study of heterogeneous catalysts used in industry and academia.

Magnus' pink salt $[Pt(NH_3)_4][PtCl_4]$, its precursors (K_2PtCl_4 and $Pt(NH_3)_4Cl_2$), and the isomeric Magnus' green salt $[Pt(NH_3)_4][PtCl_4]$ have been fully characterized by multinuclear ultra-wideline solid-state magnetic resonance (Table 7) [41]. ^{35}Cl WURST–QCPMG and BRAIN-CP/WURST–QCPMG SSNMR spectra were used to distinguish between the isomers and starting compounds (see Fig. 5). It was noted that small deviations from D_{4h} symmetry were largely responsible for the observed differences in the EFG tensor parameters amongst the compounds. Several other methods, including ^{195}Pt and ^{14}N SSNMR, powder X-ray diffraction, X-ray absorption fine structure experiments, and computational chemistry, were also used to elucidate the structure of Magnus' pink salt. Quadrupolar coupling data have been reported for the related compounds *cis*- and *trans*-$PtCl_2(NH_3)_2$[42].

^{35}Cl SSNMR allowed the confirmation of theoretically predicted NMR parameters for bridging halogen sites in a niobium chloride cluster compound $[Nb_6Cl_{12}(OH)_2(H_2O)_4{\cdot}4H_2O]$ [29]. GIPAW–DFT calculations and experimental results were in strong agreement and proved to be a powerful tool.

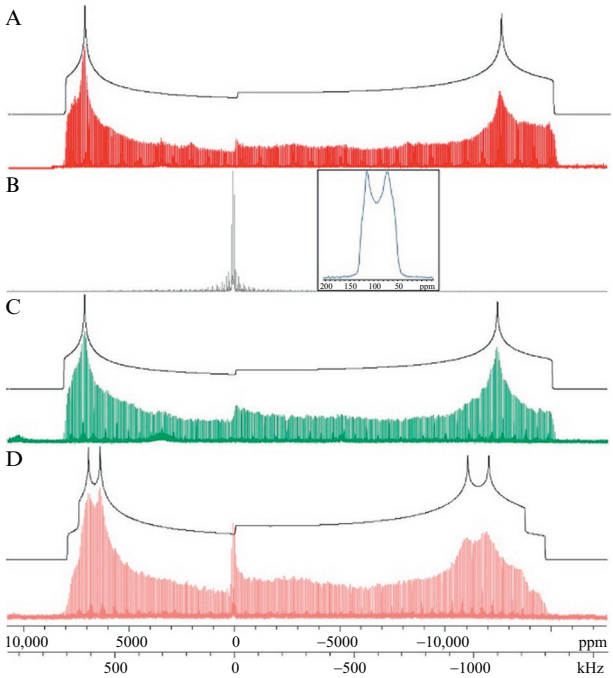

Figure 5 Static ^{35}Cl NMR spectra and their respective simulations: (A) K_2PtCl_4, (B) $Pt(NH_3)_4Cl_2{\cdot}H_2O$, (C) Magnus' green salt, and (D) Magnus' pink salt. $B_0 = 21.1$ T. *Reprinted with permission from Ref. [41]. Copyright 2014 American Chemical Society.*

Huang, Baines, and coworkers have employed ^{35}Cl SSNMR spectroscopy as an indirect probe of germanium oxidation states and coordination environments in germanium chlorides (data in Table 6) [16]. Their work followed Kroeker and coworkers' report of the ^{35}Cl CS (and $C_Q < 40$ kHz) for pure $GeCl_2$[15]. Given the challenges associated with ^{73}Ge NMR spectroscopy, ^{35}Cl is seen as a welcome alternative probe of these compounds. The quadrupolar parameters were found to be correlated to various structural metrics and to the oxidation state of germanium. In particular, correlations were observed between $C_Q(^{35}Cl)$ and the Ge–Cl bond length, the donor-Ge–Cl bond angle, and most drastically the oxidation state of germanium. Ge(IV) compounds were found to have larger $C_Q(^{35}Cl)$ (>40 MHz) values than Ge(II) compounds ($C_Q = 10$–30 MHz), although this is likely an indirect effect. Nevertheless, the findings suggest that ^{35}Cl SSNMR spectroscopy could prove to be an appealing alternative to synchrotron techniques for assessing oxidation states of main group chlorides.

Some of the above-mentioned publications on metal chlorides feature chlorine atoms involved in covalent bonds to the metals. This results in $C_Q(^{35}Cl)$ values on the order of up to ~40 MHz. It is known from NQR studies, computational chemistry, and indirect NMR methods, however, that the values of $C_Q(^{35}Cl)$ for chlorine atoms covalently bonded to carbon atoms in organic molecules are closer to ~70 MHz [2,3]. Terskikh *et al.* reported preliminary ^{35}Cl data for hexachlorophene [25]; Perras and Bryce reported direct ^{35}Cl WURST–QCPMG SSNMR experiments to measure $C_Q(^{35}Cl)$ for covalently bonded chlorine in a larger set of organic compounds (see Fig. 6 and Table 12) [11]. Due to the large size of the quadrupolar interaction relative to the Zeeman interaction, even at 21.1 T, new software was written to properly simulate the powder NMR line shapes [9,11]. Data for chlorouracil, 2-chloroacetamide (a pesticide), sodium chloroacetate, α,α'-dichloro-*o*-xylene, chlorothiazide, 2,4′-dichloroacetophenone (a diuretic), and *p*-chlorophenylalanine were simulated using the QUEST software. Despite the breadth of the spectra, the ^{35}Cl isotropic chemical shifts and quadrupolar asymmetry parameters were found to be diagnostic of the hybridization state of the directly bonded carbon atom. Resonances due to chemically distinct chlorine atoms in a molecule, as well as crystallographically distinct chlorine atoms in the crystal structure, were resolved in the spectra. The signal-to-noise obtained at 21.1 T in reasonable times suggests that systems in which the covalently bonded chlorine atoms are more dilute could be examined successfully with ^{35}Cl SSNMR.

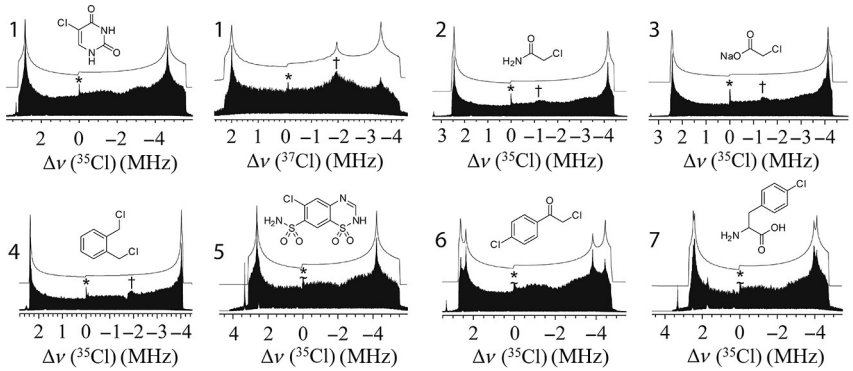

Figure 6 $^{35/37}Cl$ WURST–QCMPG NMR spectra of chlorine atoms that are covalently bonded to carbon atoms in organic compounds. Compounds **1**–**7** are 5-chlorouracil, 2-chloroacetamide, sodium chloroacetate, α,α'-dichloro-*o*-xylene, chlorothiazide, 2,4′-dichloroacetophenone, and *p*-chlorophenylalanine, respectively. *From Ref. [11]. Copyright 2012 Wiley-VCH.*

The theory of residual dipolar coupling between quadrupolar nuclei has been developed and applied to B-chlorocatecholborane using ^{11}B and $^{35/37}$Cl SSNMR [26]. MAS and DOR NMR were applied to extract information regarding the quadrupolar coupling constants, J coupling, and dipolar coupling constant for the boron–chlorine spin pair. The value of $J(^{35}\text{Cl},^{11}\text{B})_{iso}$ was reported as -30 ± 15 Hz, and this was well reproduced by computational chemistry. The boron spectra acquired at various fields were also shown to be sensitive to the relative orientation of the boron and chlorine EFG tensors. Importantly, the ^{11}B NMR spectra were also shown to be sensitive to the sign of C_Q of the coupled nucleus, i.e., ^{35}Cl.

Additional work on measuring dipolar and J coupling between quadrupolar nuclei using double-rotation NMR was reported by Perras and Bryce [27]. Amongst the compounds studied was trichloroborazine. The ^{11}B SSNMR spectra are greatly affected by coupling to the $^{35/37}$Cl nuclei, and a value of $^1J(^{35}\text{Cl},^{11}\text{B})_{iso}$ of -30 Hz was determined. Independent ^{35}Cl wideline SSNMR data for both crystallographic chlorine sites were also reported in this work (see Table 17).

A low-temperature magnetic field-swept study of the $^{63/65}$Cu and $^{35/37}$Cl NMR spectra provided insight into triplet localization in the quantum spin system NH_4CuCl_3[43]. The temperature dependencies of the spectra were also reported. $^{35/37}$Cl NMR experiments at the ¼-plateau phase found two different temperature dependencies of the Cl resonances, interpreted as being due to the transferred hyperfine field at the Cl site located at a singlet site and at a triplet site, respectively.

4. SOLID-STATE BROMINE-79/81 NUCLEAR MAGNETIC RESONANCE

Bromine-79 and bromine-81 have excellent N.A. and resonance frequencies; however, their moderately large quadrupole moments and Sternheimer antishielding factors result in much broader NMR powder patterns when compared to $^{35/37}$Cl [3]. For this reason, there are fewer studies in the literature. We remind the reader to consult our previous reviews for data published prior to 2009 [1,2,4]. Recent data for $^{79/81}$Br are summarized in Tables 18–23. An overview of some important interesting findings is presented below.

NMR crystallography refers to the use of NMR data as restraints or constraints in the refinement or solution of a crystal structure [47]. NMR data are often combined with more traditional crystallographic data, such as

Table 18 ^{81}Br solid-state NMR data for haloanilinium bromides from Attrell *et al.* [13]

Compounds	δ_{iso} (ppm)[a]	Ω (ppm)	C_Q (MHz)	η_Q	κ	Notes
2-Chloroanilinium bromide	135(3)	210(20)	37.95(30)	0.31(5)	0.2(1)	Experimental
	30.9	*203.9*	*−30.94*	*0.61*	*−0.29*	*Calculated*
2-Bromoanilinium bromide	155(10)	240(10)	38.0(2)	0.27(1)	0.0(5)	Experimental
	91.4	*213.5*	*−35.49*	*0.23*	*−0.64*	*Calculated*
2-Iodoanilinium bromide	187(5)	75(10)	12.3(2)	0.85(1)	0.2(2)	Experimental
3-Chloroanilinium bromide	130(10)	120(30)	45.3(1)	0.665 (5)	−0.7(2)	Experimental
	10.3	*179.8*	*−38.17*	*0.87*	*−0.71*	*Calculated*
3-Bromoanilinium bromide	250(10)	340(10)	27.7(2)	0.67(5)	−0.2(1)	Experimental
	91.5	*235.7*	*−14.48*	*0.68*	*0.22*	*Calculated*
4-Chloroanilinium bromide	230(10)	220(30)	26.2(1)	0.66(1)	0.4(1)	Experimental
4-Bromoanilinium bromide	100(10)		20.0(1)	1.0(1)		Site 1
	150(10)	190(20)	26.2(1)	0.92(2)	−1.0(1)	Site 2
4-Iodoanilinium bromide	*81.6*	*90.0*	*−14.10*	*0.82*	*0.08*	*Calculated*

[a]All chemical shifts were referenced to 0.01 mol/dm^3 NaBr in D_2O. Secondary standard: KBr(s) at 54.51 ppm.

Table 19 ^{81}Br SSNMR parameters for pure ionic liquid salts from Gordon *et al.* [14]

Compounds	δ_{iso} (ppm)[a]	Ω (ppm)	C_Q (MHz)	η_Q	κ
bNH_3 bromide	137.0(0.5)	75(2)	17.50(0.02)	0.01(0.01)	0.05 (0.05)
emim bromide	122(1)	73(3)	12.40(0.01)	0.28(0.01)	0.95 (0.05)
bmim bromide	172(1)	−58(2)	7.35(0.05)	0.86(0.02)	0.64 (0.10)
empyrro bromide	123(1)	51(1)	5.12(0.05)	0.37(0.08)	0.96 (0.04)

[a]All chemical shifts were referenced to 0.01 M NaBr in D_2O. See Fig. 4 for cation structures.

diffraction patterns, to find the optimum structure solution. In instances where single crystal X-ray diffraction is not possible, SSNMR parameters can be particularly valuable in providing structural information. Widdifield and Bryce reported the use of $^{79/81}$Br SSNMR spectra (and also ^{25}Mg

Table 20 ^{81}Br SSNMR parameters for halogen-bonded compounds from Viger-Gravel *et al.* [23]

Compounds[a]	δ_{iso} (ppm)[b]	Ω (ppm)	C_Q (MHz)	η_Q	κ
(*n*-Bu_4NBr)(*p*-DITFB)	250(6)	255(20)	58.0(0.2)	0.22(0.01)	1.0(0.2)
(*n*-Bu_4PBr)(*p*-DITFB)	310(10)	110(10)	57.0(0.2)	0.19(0.01)	0.9(0.3)
(*n*-Bu_4PBr)(*o*-DITFB)	256(4)	192(10)	30.8(0.1)	0.27(0.01)	0.0(0.1)
($EtPh_3PBr$)(*p*-DITFB)	210(10)	320(20)	40.7(0.1)	0.26(0.01)	0.9(0.1)
($EtPh_3PBr)_2$(*p*-DIB)	140(10)	115(15)	21.5(0.1)	0.32(0.01)	−0.9(0.2)

[a] *p*-DITFB, *para*-diiodotetrafluorobenzene; *o*-DITFB, *ortho*-diiodotetrafluorobenzene; *p*-DIB, *para*-dioodobenzene.
[b] All chemical shifts were referenced to KBr(s) (δ_{iso} = 54.51 ppm) with respect to 0.03 M NaBr in D_2O.

Table 21 ^{81}Br SSNMR parameters for *n*-alkyltrimethylammonium bromide salts $C_xH_{2x+1}(CH_3)_3N^+Br^-$ from Alonso *et al.* [44]

Compounds	MAS (kHz)	δ_{iso} (ppm)[a]	Δ_{CSA} (ppm)[b]	C_Q (MHz)	η_Q	η_{CSA}[b]
TMAB (x = 1)	14	46.1	−22	6.03	0.026	0.2
	7	45.6	−18	6.03	0.025	0.8
	0	45.4	−18	6.03	0.013	0.2
Average		45.7		6.03	0.02	
Standard Dev.		0.3		0.002	<0.01	
DTAB (x = 12)	30	59	65	7.27	0.137	0.7
	14	57	58	7.32	0.101	1.0
	7	59	70	7.53	0.099	0.3
	0	59		7.44	0.120	
Average		58.6		7.39	0.11	
Standard Dev.		0.9		0.10	0.02	
TTAB (x = 14)	30	57	64	7.57	0.131	0.6
	14	55.3	66	7.57	0.143	0.4
	7	57.2	63	7.94	0.200	0.4
	0	57.5		7.89	0.169	
Average		56.7		7.74	0.16	
Standard Dev.		0.8		0.17	0.03	

Continued

Table 21 ^{81}Br SSNMR parameters for *n*-alkyltrimethylammonium bromide salts $C_xH_{2x+1}(CH_3)_3N^+Br^-$ from Alonso *et al.* [44]—cont'd

Compounds	MAS (kHz)	δ_{iso} (ppm)	Δ_{CSA} (ppm)	C_Q (MHz)	η_Q	η_{CSA}
HTAB ($x=16$)	30	56	64	8.01	0.187	0.3
	14	55	66	8.03	0.191	0.4
	7	56	54	8.07	0.194	0.7
	0	57		8.00	0.137	
Average		55.9		8.03	0.18	
Standard dev.		0.8		0.03	0.02	
OTAB ($x=18$)	30	55	62	7.99	0.185	0.6
	14	53.4	62	8.04	0.185	0.5
	7	54.2	52	8.14	0.193	0.7
	0	54.3		8.13	0.186	
Average		54.2		8.08	0.19	
Standard dev.		0.5		0.07	<0.01	

[a]All chemical shifts were referenced to KBr(s) ($\delta_{iso}=0$ ppm) spun at 2–5 kHz.
[b]See Ref. [44] for a description of these parameters.

SSNMR data and GIPAW–DFT computations) to refine the crystal structure of $MgBr_2$[45]. $^{79/81}$Br NMR is particularly sensitive to structural changes due to its substantial quadrupole moment. This report demonstrated that NMR crystallography of inorganic compounds comprised solely of quadrupolar nuclei is feasible.

In a related study, solid-state $^{79/81}$Br NMR and GIPAW calculations were used to study structure, symmetry, and hydration state in a broader series of alkaline earth metal bromides (see Table 22) [46]. Using NMR data acquired at magnetic fields of up to 21.1 T, marked differences in the $^{79/81}$Br parameters (δ_{iso} and C_Q) were observed between the hydrates and the anhydrous materials. These differences suggest that $^{79/81}$Br SSNMR is a sensitive tool to distinguish between polymorphs and pseudopolymorphs [46]. It was also found that a point charge computational model could not reproduce the experimental data quantitatively, despite the apparent ionic nature of the crystals, and thus first-principles calculations are recommended.

As described above in the section on chlorine NMR, halogen bonds represent a fascinating class of noncovalent interaction, which can be probed via SSNMR. Viger-Gravel *et al.* report $^{79/81}$Br SSNMR data for bromide

Table 22 $^{79/81}$Br SSNMR parameters for anhydrous alkaline earth metal bromides and hydrates from Widdifield and Bryce [45,46]

Compounds	δ_{iso} (ppm)[a]	Ω (ppm)	$\lvert C_Q(^{81}Br)\rvert$ (MHz)	$\lvert C_Q(^{79}Br)\rvert$ (MHz)	η_Q	κ	Notes
$CaBr_2$	280(50)	250(150)	62.8(4)	75.1(5)	0.445(20)	0	
$CaBr_2{\cdot}xH_2O$	−55(4)	–	–	–	–	–	Site 1
	205(15)	–	12.8(4)	15.4(5)	0.32(4)	–	Site 2
	170(15)	–	23.0(4)	27.6(5)	0.25(3)	–	Site 3
$SrBr_2$	422(5)	50(20)	10.3(3)	12.3(3)	0.07(4)	−1	Site 1
	410(8)	85(25)	18.10(20)	21.65(20)	0.03(2)	−1	Site 2
	320(10)	110(30)	25.6(2)	30.6(2)	0.695(15)	0.3(4)	Site 3
	300(50)	–	53.7(6)	64.2(6)	0.33(2)	–	Site 4
$SrBr_2{\cdot}6H_2O$	95(15)	70(30)	27.7(3)	33.2(3)	<0.01	−1	
$BaBr_2$	280(10)	200(20)	23.5(3)	28.1(4)	0.17(2)	−0.6(2)	Site 1
	480(15)	170(30)	27.2(3)	32.5(3)	0.070(15)	0.1(2)	Site 2
$BaBr_2{\cdot}2H_2O$	218.2(1.0)	86(5)	7.32(3)	8.74(4)	0.76(2)	−0.20(0.15)	
$MgBr_2{\cdot}6H_2O$	57(7)	50(20)	19.0(2)	22.7(2)	0.23(3)	0.7(0.3)	
$MgBr_2$	285(10)	–	21.93(0.20)	26.25(0.20)	0.02(2)		

[a]All chemical shifts were referenced to KBr(s) ($\delta_{iso}=0$ ppm).

Table 23 $^{79/81}$Br SSNMR parameters for phosphonium bromides from Burgess *et al.* [30]

Compounds	δ_{iso} (ppm)[a]	Ω (ppm)	$C_Q(^{81}Br)$ (MHz)	η_Q	κ	Notes
$BrBuPPh_3$	130.5(5)	99(5)	9.48(0.10)	0.54(0.07)	0(0.05)	Experimental
	54.6	*151*	*−9.35*	*0.79*	*0.06*	*Calculated*
$BrPrPPh_3$	121(2)	105(5)	8.48(0.20)	0.56(0.03)	−0.35(0.10)	Experimental
	25.4	*162*	*−8.98*	*0.59*	*−0.01*	*Calculated*
$BrEtPPh_3$	151(1)	160(10)	14.00(0.10)	0.52(0.02)	−0.80(0.10)	Experimental
	87.9	*292*	*−10.78*	*0.84*	*−0.78*	*Calculated*
$BrMePPh_3$	155(2)	98(3)	9.80(0.15)	0.26(0.01)	0.60(0.05)	Experimental
	47.3	*156*	*6.74*	*0.34*	*−0.53*	*Calculated*
$Br(C_5H_9)PPh_3$	82(1)	140(10)	12.80(0.10)	0.62(0.01)	0.50(0.20)	Experimental
	3.4	*314*	*−65.52*	*0.24*	*−0.42*	*Calculated*
$BrHPPh_3$	228(5)	305(10)	14.35(0.10)	<0.01	0.55(0.05)	Experimental
	359.8	*726*	*−74.85*	*0.00*	*0.85*	*Calculated*
$BrPPh_4$/site a	3(1)	–	10.50(0.05)	0.48(0.02)	–	Experimental
	−88.3	*257*	*13.20*	*0.28*	*0.19*	*Calculated*
$BrPPh_4$/site b	46(1)	–	8.55(0.05)	0.57(0.02)	–	Experimental
	16.0	*365*	*12.20*	*0.34*	*0.32*	*Calculated*

[a]All chemical shifts were referenced to KBr(s) (^{79}Br δ_{iso} = 54.31 ppm, ^{81}Br δ_{iso} = 54.51 ppm).

anions that act as halogen bond acceptors in a series of halogen-bonded co-crystals formed between *para*-diiodotetrafluorobenzene (*p*-DITFB), *ortho*-diiodotetrafluorobenzene (*o*-DITFB), *para*-diiodobenzene (*p*-DIB), and phosphonium or ammonium bromide salts (see Table 20) [23]. Accompanied by a thorough NLMO study, these measurements allowed the authors to gain insights into the chemical and electronic environments of the halogen bond. The results show a correlation between the NMR parameters and the halogen bond geometry. Representative ^{81}Br bromine SSNMR spectra are shown in Fig. 7. The $^{79/81}$Br data of Attrell *et al.* for halogen-bonded haloanilium bromides are presented in Table 18 [13]. In that study, a correlation between the bromine CS (and CSA) and the halogen bond length was noted.

Five *n*-alkyltrimethylammonium bromide $C_xH_{2x+1}(CH_3)_3N^+Br^-$ salts ($x=1$, 12, 14, 16, 18) were characterized by ^{14}N and ^{81}Br MAS SSNMR in order to determine their NMR parameters and provide insight into their crystal structures (Table 21) [44]. Diffraction data and computations were also used in a complementary manner. The combined use of both ^{14}N and ^{81}Br NMR data proved to be useful for structure refinement due to the fact that the NMR parameters were found to be strongly dependent on the chain packing among the five samples, more specifically variations in C–N–C angles and in the spatial positioning of the cations and anions.

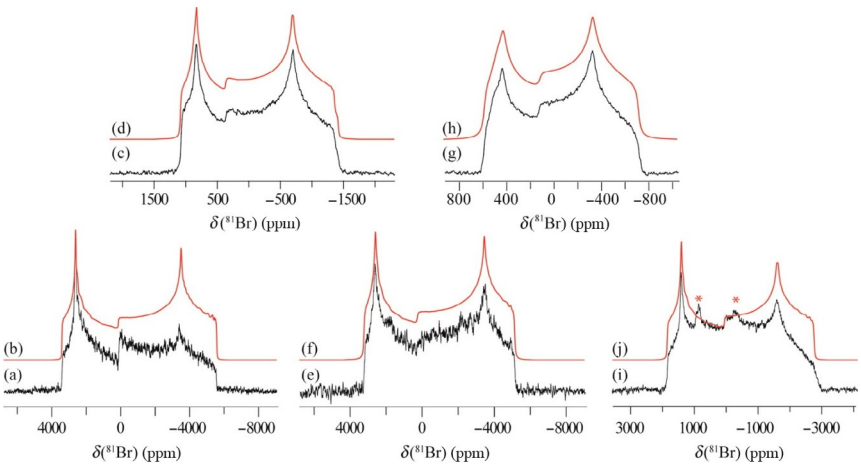

Figure 7 Representative ^{81}Br solid-state NMR spectra of halogen-bonded compounds ($B_0=21.1$ T). The compounds are (a) (n-Bu_4NBr)(*p*-DITFB), (c) (n-Bu_4PBr)(*o*-DITFB), (e) (n-Bu_4PBr)(*p*-DITFB), (g) $(EtPh_3PBr)_2$(*p*-DIB), (i) ($EtPh_3PBr$)(*p*-DITFB), and their simulated spectra are (b), (d), (f), (h), and (j), respectively. The asterisks in (i) mark an impurity. *Reprinted with permission from Ref. [23]. Copyright 2014 American Chemical Society.*

A series of seven different triphenylphosphonium bromide compounds were characterized using $^{79/81}$Br and ^{31}P SSNMR in order to determine their EFG and chemical shift tensors (see Table 23) [30]. The $^{79/81}$Br NMR parameters, in particular the chemical shift tensor component δ_{11}, were shown to be dependent on the Br–P distance, and thus this parameter may be useful in NMR crystallographic structure refinements. Due to inconsistencies with the NMR data, a correction to the existing X-ray diffraction crystal structure of $BrPPh_4$ was presented [30]. All GIPAW–DFT calculations on the other crystal structures seem to be in accordance with experimental results.

In their report on the development and implementation of a fast graphical program for the exact simulation of NMR and NQR spectra for quadrupolar nuclei (QUEST), Perras *et al.* used $^{79/81}$Br NMR spectra acquired for powdered $CaBr_2$ for validation [9]. The program employs full diagonalization of the combined Zeeman-quadrupolar Hamiltonian and can simulate NMR spectra over the full regime of ν_0 and ν_Q ratios. $^{79/81}$Br SSNMR spectra acquired in magnetic fields ranging from 4.7 to 21.1 T revealed the breakdown of the high-field approximation for quadrupolar nuclei, showing that second-order perturbation theory is not sufficient in certain cases. For example, the low-frequency discontinuity of the $^{79/81}$Br powder pattern for $CaBr_2$ was shown to deviate by 1.4 MHz from that predicted by second-order perturbation theory in a magnetic field of 4.7 T (see Fig. 8).

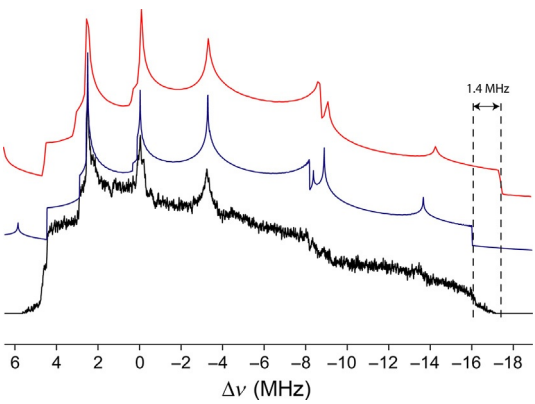

Figure 8 $^{79/81}$Br NMR spectrum of $CaBr_2$ acquired at 4.7 T along with an exact simulation (blue (dark gray in the print version; middle trace)) and second-order perturbation theory simulation (red (gray in the print version; top trace)). At this field, none of the singularities are well reproduced by second-order perturbation theory although the discrepancy is more pronounced at the low-frequency end of the spectrum where there is a difference of 1.4 MHz between the two simulations. *From Ref. [9]. Copyright 2012 Elsevier. Used with permission.*

^{11}B SSNMR and $^{79/81}$Br NQR studies of B-bromocatecholborane provided a wealth of data on the boron site, the bromine site, and the coupling between the relevant nuclei ($C_Q(^{81}Br) = 290.7$ MHz; $\eta_Q = 0.25$) [27]. ^{11}B DOR NMR spectra in particular provided information on spin–spin coupling between ^{11}B and $^{79/81}$Br. The value of $J_{iso}(^{81}Br,^{11}B)$ was found experimentally to be -75 Hz, and the anisotropy, ΔJ, was measured as 500 Hz. These data are particularly interesting as couplings between quadrupolar nuclei are rare and are not often easily measurable; indeed this is probably the first report of anisotropic J coupling between quadrupolar nuclei in the solid state.

The ^{79}Br SSNMR CS and spin–lattice relaxation time constant of KBr has been shown to be dependent on the sample temperature during MAS experiments due to the rapid rotation and sample irradiation [48]. This phenomenon is a reliable tool to determine the sample temperature under MAS conditions where it would otherwise be difficult to probe the temperature using conventional methods because of the temperature difference between the interior and exterior of the rotor. A modified method to account for magnetic field instability has also been reported [49].

As an alternative to using KBr to determine sample temperature, semiconductor quantum dots may be used to determine the temperature [50]. The material can be deposited on the outside of a rotor, and temperature readings can be obtained during NMR experiments. The setup requires special photoluminescent equipment to excite the material and determine the temperature. On the other hand, quantum dots have the advantages of not introducing KBr into samples and of being more accurate at temperatures above 250 K. Quantum dots are recommended for experiments above 50 K, whereas ^{79}Br seems to be more reliable for experiments below 50 K due to the low sensitivity of λ_{PL} of the quantum dots at low temperatures [50].

Through a combined solution NMR relaxation and computational study, Gryff-Keller *et al.* have reported on the magnetic moments of the two bromine isotopes, and they discussed the value for the absolute shielding constant of the bromide anion, 3434 ppm [51].

5. SOLID-STATE IODINE-127 NUCLEAR MAGNETIC RESONANCE

Iodine-127 has 100% N.A. and a relatively high magnetogyric ratio (see Table 1). Due to its large quadrupole moment and Sternheimer antishielding factor, broad powder patterns are typically obtained for ^{127}I in noncubic solids [3]. For a given chemical environment, the lines are much

Table 24 ^{127}I solid-state NMR data for metal iodides from Widdifield and Bryce [7]

Compounds		δ_{iso} (ppm)[a]	$\lvert C_Q(^{127}I)\rvert$ (MHz)	η_Q	Additional comments
MgI_2[b]		920(50)	79.8(0.5)	0.02(0.02)	
CaI_2		755(10)	43.5(0.3)	0.02(0.02)	
SrI_2	Site 1	880(70)	105.2(0.7)	0.467(0.012)	
	Site 2	720(150)	214.0(0.1)	0.316(0.002)	
BaI_2	Site 1[b]	650(70)	96.2 (0.8)	0.175(0.015)	
	Site 2	1000(80)	120.9 (0.2)	0.015(0.015)	
CdI_2 (4H)		1450(100)	95.7 (1.0)	0	One-site model
CdI_2 (4H)	Site 1	1450(100)	95.7 (1.0)	0	Two-site model
	Site 2	1420(100)	97.5 (1.0)	0	
$BaI_2{\cdot}2H_2O$[c]		630(20)	53.8(0.3)	0.53(0.01)	$T=295$ K
		630	52.4(0.3)	0.56(0.01)	$T\approx243$ K
$SrI_2{\cdot}6H_2O$		440(25)	133.6(0.1)	<0.01	

[a]All chemical shifts were referenced to 0.1 mol/dm^3 KI in D_2O at 0 ppm using solid NaI or KI as secondary standards (δ_{iso} (NaI) = 226.71 ppm, δ_{iso} (KI) = 192.62 ppm).
[b]MgI_2: $\Omega=120(80)$ ppm; $\kappa=-1$. BaI_2, site 1: $\Omega=300(100)$; $\kappa<-0.5$. See original reference for further information.
[c]$BaI_2{\cdot}2H_2O$: $\Omega=60(15)$ ppm; $\kappa>0.5$. See original reference for further information.

broader than those for $^{79/81}$Br, which are already much broader than those for $^{35/37}$Cl. For this reason, ^{127}I SSNMR spectra are often challenging to acquire. They can also be challenging to interpret due to the breakdown of second-order perturbation theory as discussed above [7]. The highest possible applied magnetic field is therefore desirable. An alternative is ^{127}I NQR [52] should only quadrupolar information be desired, and if one is willing to spend the time searching for the NQR signals. Newly reported ^{127}I SSNMR data are presented in Tables 24 and 25; some discussion of recent studies is provided below.

A solid-state ^{127}I NMR and GIPAW–DFT study of metal iodides and their hydrates reports on the insights available into structure, symmetry, and higher-order quadrupole-induced effects (see Fig. 1 and Table 24) [7]. Measurements of the ^{127}I SSNMR parameters at 21.1 T of anhydrous group 2 metal iodides, hydrates, and CdI_2 (4H polytype) were presented

Table 25 ^{127}I solid-state NMR data for additional compounds

Compounds	δ_{iso} (ppm)	Ω (ppm)	$\lvert C_Q(^{127}I)\rvert$ (MHz)	η_Q	References	Additional comments
1a·2H_2O[a]	250(30)	–	49.2(0.5)	0.97(0.03)	Widdifield *et al.* [37]	VOCS Solomon echo
2a·2H_2O[a]	250(60)	–	48(2)	0.19(0.05)	Widdifield *et al.* [37]	
P3[b]	380(40)	–	84.8(0.6)	0.04(0.02)	Widdifield *et al.* [37]	
PbI_2[c]	298	–	23.173	0	Taylor *et al.* [53]	T=253 K
	340	–	20.991	0		T=298 K
	356	–	18.787	0		T=343 K
2-Chloroanilinium iodide[d]	340(10)	300(100)	57.50(75)	0.775(20)	Attrell *et al.* [13]	
2-Bromoanilinium iodide[d]	500(50)	<1000	152.50(25)	0.235(20)	Attrell *et al.* [13]	
tmim iodide[e]	143(18)	0	36.8(0.9)	0.73(0.01)	Gordon *et al.* [14]	
dmpyrro iodide[e]	282.0(0.7)	184(3)	16.9(0.1)	0.27(0.02)	Gordon *et al.* [14]	
GeI_2	445(5)[f]	250(25)	8.0(0.5)	0	Greer *et al.* [15]	

[a]Alkylammonium iodides (see Ref. [37]), referenced using KI(s) (δ_{iso} = 192.62 ppm).
[b]Halogen-bonded adduct of **1a** (see Ref. [37]), referenced using KI(s) (δ_{iso} = 192.62 ppm).
[c]Variable temperature experiment, referenced using the unified Ξ scale (0.01 M KI in D_2O versus ^{1}H resonance of dilute TMS in $CDCl_3$).
[d]Compounds were referenced using 0.01 mol/dm^3 KI in D_2O; secondary standard was KI(s) at 192.62 ppm.
[e]Compounds were referenced with 0.01 M KI in D_2O. See Fig. 4 for cation structures.
[f]Referenced to KI(s) at 0 ppm.

and compared to results obtained from GIPAW–DFT calculations. In the cases where the compounds had $C_Q(^{127}I)$ values lower than 120 MHz, it was possible to also acquire data at 11.75 T and combine them with those available at 21.1 T. In such cases, the iodine chemical shift tensor spans were measured to range between 60 ppm in $BaI_2{\cdot}H_2O$ and 300 ppm in BaI_2. These measurements mark the first full characterization of ^{127}I NMR parameters (quadrupolar and CS tensors) for noncubic iodine compounds by SSNMR. However, in unfavorable cases, for instance if the value of C_Q is greater than 120 MHz, not all the information could be extracted due to the unreliability of second-order perturbation theory. These advancements show the potential that ^{127}I can have for probing the electronic environment of iodine compounds, as well as its potential application in crystallography [7]. The work also prompted the further investigation of higher-order quadrupole effects and the development of software to treat the situation exactly [8,9].

Halogen-bonded complexes formed between decamethonium diiodide (i.e., $[(CH_3)_3N^+(CH_2)_{10}N^+(CH_3)_3][2I^-]$) and various *para*-dihalogen-substituted benzene moieties (i.e., p-$C_6X_2Y_4$, X = Br, I; Y = H, F) were characterized by SSNMR (^{13}C, $^{14/15}N$, ^{19}F, and ^{127}I); see Fig. 9 [37]. Despite the challenges of acquiring the ^{127}I SSNMR spectra, structural information was obtained and NMR parameters were reported (see Table 25). Comparison between experimental and GIPAW–DFT computational results shows that

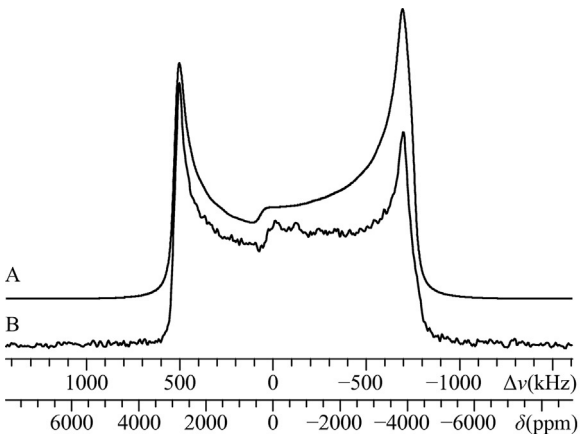

Figure 9 (a) Best-fit analytical simulation and (b) experimental VOCS Solomon echo ^{127}I $\{^1H\}$ NMR spectrum of a halogen-bonded *p*-diiodobenzene–decamethonium diiodide complex, acquired at 21.1 T. *From Ref. [37]. Copyright 2013 Wiley-VCH. Used with permission.*

halogen bonding can strongly affect the NMR parameters of ^{127}I as well as the other nuclei involved. Experimental ^{127}I SSNMR measurements showed an increase in the value of $C_Q(^{127}I)$ for the iodide anion upon formation of a halogen bond, consistent with the notion that the formation of a halogen bond perturbs the high electronic symmetry of an isolated iodide anion.

The crystal structure of lead iodide (PbI_2) has a significant number of vacancies. PbI_2 has been characterized by ^{127}I and ^{207}Pb SSNMR in order to understand the structure of the compound as well as its nuclear spin–lattice relaxation [53]. The study yielded information on the NMR parameters at different temperatures and found that the quadrupolar coupling and CS of ^{127}I are both linearly dependent on the sample temperature. It was reported that the spin–lattice relaxation below 300 K is dominated by a lattice vibration-induced modulation of EFGs, whereas above 300 K, a thermally activated mechanism associated with random hopping of iodide ions causes additional relaxation.

Yesinowski *et al.* have reported on a study of the electrical and ionic conductivity effects on the NMR parameters of CuI [54]. As a result of the Lorentz force, the rapid spinning of copper halides in a strong magnetic field causes electrical currents to be generated within the sample. This results in heating of the sample and an MAS rate dependence of the CSs. The authors show that this phenomenon is explained by resistive heating from oscillating electric currents induced along the rotor axis. The authors also report the ^{127}I CS dependence on sample temperature, about 0.27 ppm/K, but note that this depends on the particular sample and its source.

Kroeker and coworkers reported the ^{127}I NMR parameters for GeI_2, and from MAS NMR spectra were able to determine the value of $^1J(^{127}I, ^{73}Ge)$ as 35 ± 10 Hz [15]. This is a rare experimental example of a J coupling involving ^{127}I, and it is also a rare example of a coupling between two quadrupolar nuclei. The reduced coupling constant was determined to be consistent with those involving other group 14 halides.

A combined $^{69/71}$Ga SSNMR and ^{127}I NQR study of the synthetic reagent known as "GaI" elucidated its precise composition [55]. Although no ^{127}I SSNMR spectra are reported, the gallium NMR data as well as the ^{127}I quadrupolar frequencies determined from NQR allowed for "GaI" to be identified as two equivalents of Ga^0 metal with two equivalents of GaI_2, where the latter is composed of Ga^+ and GaI_4^- ions. The NMR and NQR data therefore suggest the following formulation: $[Ga^0]_2[Ga]^+[GaI_4]^-$.

Finally, we briefly mention a study that examined relativistic effects on the nuclear magnetic resonance shielding of FX (X = F, Cl, Br, I, and At)

molecular systems [56]. *Ab initio* full four-component and spin-free calculations of the NMR shielding parameters of these molecules were performed and the role of relativity assessed. The paramagnetic shielding along the bond axis, $\sigma_{||}^{P}$, which is zero in the nonrelativistic Ramsey theory [57], was calculated to be −447.4 ppm for ^{127}I in FI. This work nicely highlights the importance of considering relativistic effects in the calculation and interpretation of the NMR parameters particularly of iodine, but also bromine. The breakdown of Flygare's nonrelativistic formula [58] relating spin–rotation constants and magnetic shielding constants is discussed in the context of their results.

6. CONCLUDING REMARKS

Numerous advances have been reported in the past several years in the field of chlorine, bromine, and iodine SSNMR spectroscopy. As in the past, an increasing availability of high-field NMR instrumentation and new experimental methods have contributed to these advances. Unsurprisingly, most of the new experimental data are for the ^{35}Cl and ^{37}Cl isotopes, due to the manageable size of their quadrupole moments. Nevertheless, the measurement of new bromine and iodine data have been instrumental in providing insight into a variety of compound classes including halogen-bonded adducts, ionic liquids, and simple inorganic compounds. Consideration of the new chlorine NMR data expands this list to include transition metal organometallic complexes, hydrochloride salts of pharmaceuticals, and glasses, for instance. Chlorine-35/37 spectroscopy of covalently bonded chlorine atoms, both in inorganic and organic compounds, is now feasible in the solid state, but proper interpretation will often require an exact treatment of the Zeeman-quadrupole Hamiltonian. This point is more generally applicable to ^{127}I SSNMR spectra. MAS NMR, double-rotation NMR, as well as some indirect methods, have enabled the measurement of spin–spin coupling constants, including anisotropies in select cases, involving the quadrupolar halogens. Such measurements remain quite rare.

In light of the exciting technical advances as well as applications of chlorine, bromine, and iodine SSNMR described in this *Annual Report*, new developments in this area are expected to continue apace in the coming years. Continued availability of high-field SSNMR spectrometers as well as the development of improved broadband excitation methods will encourage further work in this area.

ACKNOWLEDGMENTS

We are grateful to the Natural Sciences and Engineering Research Council (NSERC) for funding. We thank Professor Ray Dupree for providing a preprint of Ref. [24].

REFERENCES

1. D.L. Bryce, G.D. Sward, Solid-state NMR spectroscopy of the quadrupolar halogens: chlorine-35/37, bromine-79/81, and iodine-127, Magn. Reson. Chem. 44 (2006) 409–450.
2. C.M. Widdifield, R.P. Chapman, D.L. Bryce, Chlorine, bromine, and iodine solid-state NMR spectroscopy, Annu. Rep. Nucl. Magn. Reson. Spectrosc. 66 (2009) 195–327.
3. D.L. Bryce, C.M. Widdifield, R.P. Chapman, R.J. Attrell, Chlorine, bromine, and iodine solid-state NMR, eMagRes (2011), http://dx.doi.org/10.1002/9780470034590.emrstm1214.
4. R.P. Chapman, C.M. Widdifield, D.L. Bryce, Solid-state NMR of quadrupolar halogen nuclei, Prog. Nucl. Magn. Reson. Spectrosc. 55 (2009) 215–237.
5. B.J. Butler, J.M. Hook, J.B. Harper, Recent advances in the NMR spectroscopy of chlorine, bromine and iodine, Annu. Rep. Nucl. Magn. Reson. Spectrosc. 73 (2011) 63–82.
6. R.K. Harris, E.D. Becker, S.M. Cabral De Menezes, P. Granger, R.E. Hoffman, K.W. Zilm, Further conventions for NMR shielding and chemical shifts (IUPAC recommendations 2008), Pure Appl. Chem. 80 (2008) 59–84.
7. C.M. Widdifield, D.L. Bryce, Solid-state ^{127}I NMR and GIPAW DFT study of metal iodides and their hydrates: structure, symmetry, and higher-order quadrupole-induced effects, J. Phys. Chem. A 114 (2010) 10810–10823.
8. C.M. Widdifield, A.D. Bain, D.L. Bryce, Definitive solid-state $^{185/187}$Re NMR spectral evidence for and analysis of the origin of high-order quadrupole-induced effects for $I=5/2$, Phys. Chem. Chem. Phys. 13 (2011) 12413–12420.
9. F.A. Perras, C.M. Widdifield, D.L. Bryce, QUEST—QUadrupolar Exact SofTware: a fast graphical program for the exact simulation of NMR and NQR spectra for quadrupolar nuclei, Solid State Nucl. Magn. Reson. 45–46 (2012) 36–44.
10. See http://mysite.science.uottawa.ca/dbryce/soft.html.
11. F.A. Perras, D.L. Bryce, Direct investigation of covalently bound chlorine in organic compounds by solid-state ^{35}Cl NMR spectroscopy and exact spectral line-shape simulations, Angew. Chem. Int. Ed. 51 (2012) 4227–4230.
12. M. Hildebrand, H. Hamaed, A.M. Namespetra, J.M. Donohue, R. Fu, I. Hung, Z. Gan, R.W. Schurko, ^{35}Cl Solid-state NMR of HCl salts of active pharmaceutical ingredients: structural prediction, spectral fingerprinting and polymorph recognition, CrystEngComm 16 (2014) 7334–7356.
13. R.J. Attrell, C.M. Widdifield, I. Korobkov, D.L. Bryce, Weak halogen bonding in solid haloanilinium halides probed directly via chlorine-35, bromine-81, and iodine-127 NMR spectroscopy, Cryst. Growth Des. 12 (2012) 1641–1653.
14. P.G. Gordon, D.H. Brouwer, J.A. Ripmeester, Probing the local structure of pure ionic liquid salts with solid- and liquid-state NMR, ChemPhysChem 11 (2010) 260–268.
15. B.J. Greer, V.K. Michaelis, V.V. Terskikh, S. Kroeker, Reconnaissance of diverse structural and electronic environments in germanium halides by solid-state ^{73}Ge NMR and quantum chemical calculations, Can. J. Chem. 89 (2011) 1118–1129.
16. M.A. Hanson, V.V. Terskikh, K.M. Baines, Y. Huang, Chlorine-35 solid-state NMR spectroscopy as an indirect probe of germanium oxidation state and coordination environment in germanium chlorides, Inorg. Chem. 53 (2014) 7377–7388.

17. C.M. Widdifield, D.L. Bryce, A multinuclear solid-state magnetic resonance and GIPAW DFT study of anhydrous calcium chloride and its hydrates, Can. J. Chem. 89 (2011) 754–763.
18. G.H. Penner, R. Webber, L.A. O'Dell, A multinuclear NMR and quantum chemical study of solid trimethylammonium chloride, Can. J. Chem. 89 (2011) 1036–1046.
19. R.P. Chapman, J.R. Hiscock, P.A. Gale, D.L. Bryce, A solid-state $^{35/37}$Cl NMR study of a chloride ion receptor and a GIPAW-DFT study of chlorine NMR interaction tensors in organic hydrochlorides, Can. J. Chem. 89 (2011) 822–834.
20. A.J. Rossini, R.W. Mills, G.A. Briscoe, E.L. Norton, S.J. Geier, I. Hung, S. Zheng, J. Autschbach, R.W. Schurko, Solid-state chlorine NMR of group IV transition metal organometallic complexes, J. Am. Chem. Soc. 131 (2009) 3317–3330.
21. R.P. Chapman, D.L. Bryce, Application of multinuclear magnetic resonance and gauge-including projector-augmented-wave calculations to the study of solid group 13 chlorides, Phys. Chem. Chem. Phys. 11 (2009) 6987–6998.
22. K.E. Johnston, C.A. O'Keefe, R.M. Gauvin, J. Trébosc, L. Delevoye, J.-P. Amoureux, N. Popoff, M. Taoufik, K. Oudatchin, R.W. Schurko, A study of transition-metal organometallic complexes combining ^{35}Cl solid-state NMR spectroscopy and ^{35}Cl NQR spectroscopy and first-principles DFT calculations, Chem. Eur. J. 19 (2013) 12396–12414.
23. J. Viger-Gravel, S. Leclerc, I. Korobkov, D.L. Bryce, Direct investigation of halogen bonds by solid-state multinuclear magnetic resonance spectroscopy and molecular orbital analysis, J. Am. Chem. Soc. 136 (2014) 6929–6942.
24. A. Baasner, I. Hung, T.F. Kemp, R. Dupree, B.C. Schmidt, S.L. Webb, Constraints on the incorporation mechanism of chlorine in peralkaline and peraluminous Na_2O–CaO–Al_2O_3–SiO_2 glasses, Am. Mineral. 99 (2014) 1713–1723.
25. V.V. Terskikh, S.J. Lang, P.G. Gordon, G.D. Enright, J.A. Ripmeester, ^{13}C CP MAS NMR of halogenated (Cl, Br, I) pharmaceuticals at ultrahigh magnetic fields, Magn. Reson. Chem. 47 (2009) 398–406.
26. F.A. Perras, D.L. Bryce, Residual dipolar coupling between quadrupolar nuclei under magic-angle spinning and double-rotation conditions, J. Magn. Reson. 213 (2011) 82–89.
27. F.A. Perras, D.L. Bryce, Measuring dipolar and *J* coupling between quadrupolar nuclei using double-rotation NMR, J. Chem. Phys. 138 (2013) 174202.
28. F.G. Vogt, G.R. Williams, R.C.B. Copley, Solid-state NMR analysis of a boron-containing pharmaceutical hydrochloride salt, J. Pharm. Sci. 102 (2013) 3705–3716.
29. B. Perić, R. Gautier, C.J. Pickard, M. Bosiočić, M.S. Grbić, M. Požek, Solid-state NMR/NQR and first-principles study of two niobium halide cluster compounds, Solid State Nucl. Magn. Reson. 59–60 (2014) 20–30.
30. K.M.N. Burgess, I. Korobkov, D.L. Bryce, A combined solid-state NMR and X-ray crystallography study of the bromide ion environments in triphenylphosphonium bromides, Chem. Eur. J. 18 (2012) 5748–5758.
31. D.L. Bryce, G.D. Sward, S. Adiga, Solid-state $^{35/37}$Cl NMR spectroscopy of hydrochloride salts of amino acids implicated in chloride ion transport channel selectivity: opportunities at 900 MHz, J. Am. Chem. Soc. 128 (2006) 2121–2134.
32. D.L. Bryce, G.D. Sward, Chlorine-35/37 NMR spectroscopy of solid amino acid hydrochlorides: refinement of hydrogen-bonded proton positions using experiment and theory, J. Phys. Chem. B 110 (2006) 26461–26470.
33. R.P. Chapman, D.L. Bryce, A high-field $^{35/37}$Cl NMR and quantum chemical investigation of the chlorine quadrupolar and chemical shift tensors in amino acid hydrochlorides, Phys. Chem. Chem. Phys. 9 (2007) 6219–6230.
34. H. Hamaed, J.M. Pawlowski, B.F.T. Cooper, R. Fu, S.H. Eichhorn, R.W. Schurko, Application of solid-state ^{35}Cl NMR to the structural characterization of hydrochloride pharmaceuticals and their polymorphs, J. Am. Chem. Soc. 130 (2008) 11056–11065.

35. D.L. Bryce, M. Gee, R.E. Wasylishen, High-field chlorine NMR spectroscopy of solid organic hydrochloride salts: a sensitive probe of hydrogen bonding environment, J. Phys. Chem. A 105 (2001) 10413–10421.
36. F.G. Vogt, G.R. Williams, M.N. Johnson, R.C.B. Copley, A spectroscopic and diffractometric study of polymorphism in ethyl 3-{3-[((2r)-3-{[2-(2,3-dihydro-1*h*-inden-2yl)-1,1-dimethylethyl]amino}-2-hydroxypropyl)oxy]-4,5-difluorophenyl}propanoate hydrochloride, Cryst. Growth Des. 13 (2013) 5353–5367.
37. C.M. Widdifield, G. Cavallo, G.A. Facey, T. Pilati, J. Lin, P. Metrangolo, G. Resnati, D.L. Bryce, Multinuclear solid-state magnetic resonance as a sensitive probe of structural changes upon the occurrence of halogen bonding in co-crystals, Chem. Eur. J. 19 (2013) 11949–11962.
38. D.L. Bryce, J. Viger-Gravel, Solid-state NMR study of halogen-bonded adducts. Top. Curr. Chem. (2014), http://dx.doi.org/10.1007/128_2014_542 (in press).
39. P. Mania, S. Conrad, R. Verel, C. Hammond, I. Hermans, Thermal restructuring of silica-grafted—CrO_2Cl and $VOCl_2$ species, Dalton Trans. 42 (2013) 12725–12732.
40. P. Mania, R. Verel, F. Jenny, C. Hammond, I. Hermans, Thermal restructuring of silica-grafted $TiCl_x$ species and consequences for epoxidation catalysis, Chem. Eur. J. 19 (2013) 9849–9858.
41. B.E.G. Lucier, K.E. Johnston, W. Xu, J.C. Hanson, S.D. Senanayake, S. Yao, M.W. Bourassa, M. Srebro, J. Autschbach, R.W. Schurko, Unravelling the structure of Magnus' pink salt, J. Am. Chem. Soc. 136 (2014) 1333–1351.
42. B.E.G. Lucier, A.R. Reidel, R.W. Schurko, Multinuclear solid-state NMR of square-planar platinum complexes—cisplatin and related systems, Can. J. Chem. 89 (2011) 919–937.
43. H. Inoue, S. Tani, S. Hosoya, K. Inokuchi, T. Fujiwara, T. Saito, T. Suzuki, A. Oosawa, T. Goto, M. Fujisawa, H. Tanaka, T. Sasaki, S. Awaji, K. Watanabe, N. Koboyashi, $^{63/65}$Cu- and $^{35/37}$Cl-NMR studies of triplet localization in the quantum spin system NH_4CuCl_3, Phys. Rev. B 79 (2009) 174418.
44. B. Alonso, D. Massiot, P. Florian, H.H. Paradies, P. Gaveau, T. Mineva, ^{14}N and ^{81}Br quadrupolar nuclei as sensitive NMR probes of *n*-alkyltrimethylammonium bromide crystal structures. An experimental and theoretical study, J. Phys. Chem. B 113 (2009) 11906–11920.
45. C.M. Widdifield, D.L. Bryce, Crystallographic structure refinement with quadrupolar nuclei: a combined solid-state NMR and GIPAW DFT example using $MgBr_2$, Phys. Chem. Chem. Phys. 11 (2009) 7120–7122.
46. C.M. Widdifield, D.L. Bryce, Solid-state $^{79/81}$Br NMR and gauge-including projector-augmented wave study of structure, symmetry, and hydration state in alkaline earth metal bromides, J. Phys. Chem. A 114 (2010) 2102–2116.
47. R.K. Harris, R.E. Wasylishen, M.J. Duer (Eds.), NMR Crystallography, Wiley, Chichester, 2009.
48. K.R. Thurber, R. Tycko, Measurement of sample temperatures under magic-angle spinning from the chemical shift and spin–lattice relaxation rate of ^{79}Br in KBr powder, J. Magn. Res. 196 (2009) 84–87.
49. R.N. Purusottam, G. Bodenhausen, P. Tekely, Determination of sample temperature in unstable static fields by combining solid-state ^{79}Br and ^{13}C NMR, J, Magn. Reson. 246 (2014) 69–71.
50. R. Tycko, Remote sensing of sample temperatures in nuclear magnetic resonance using photoluminescence of semiconductor quantum dots, J. Magn. Reson. 244 (2014) 64–67.
51. A. Gryff-Keller, S. Molchanov, A. Wodyński, Scalar relaxation of the second kind—a potential source of information on the dynamics of molecular movements. 2. Magnetic dipole moments and magnetic shielding of bromine nuclei, J. Phys. Chem. A 118 (2014) 128–133.

52. E.A.C. Lucken, Nuclear Quadrupole Coupling Constants, Academic Press, London, 1969.
53. R.E. Taylor, P.A. Beckmann, S. Bai, C. Dybowski, ^{127}I and ^{207}Pb solid-state NMR spectroscopy and nuclear spin relaxation in PbI_2: a preliminary study, J. Phys. Chem. C 118 (2014) 9143–9153.
54. J.P. Yesinowski, H.D. Ladouceur, A.P. Purdy, J.B. Miller, Electrical and ionic conductivity effects on magic-angle spinning nuclear magnetic resonance parameters of CuI, J. Chem. Phys. 133 (2010) 234509.
55. C.M. Widdifield, T. Jurca, D.S. Richeson, D.L. Bryce, Using $^{69/71}$Ga solid-state NMR and ^{127}I NQR as probes to elucidate the composition of "GaI", Polyhedron 35 (2012) 96–100.
56. S.S. Gómez, G.A. Aucar, Relativistic effects on the nuclear magnetic resonance shielding of FX (X = F, Cl, Br, I, and At) Molecular Systems, J. Chem. Phys. 134 (2011) 204314.
57. N.F. Ramsey, Magnetic shielding of nuclei in molecules, Phys. Rev. 78 (1950) 699–703.
58. (a) W.H. Flygare, Spin–rotation interaction and magnetic shielding in molecules, J. Chem. Phys. 41 (1964) 793–800. (b) T.D. Gierke, W.H. Flygare, An empirical evaluation of the individual elements in the nuclear diamagnetic shielding tensor by the atom dipole methodology, J. Am. Chem. Soc. 94 (1972) 7277–7283. (c) D.L. Bryce, R.E. Wasylishen, Microwave spectroscopy and nuclear magnetic resonance spectroscopy—what is the connection? Acc. Chem. Res. 36 (2003) 327–334.